Comparison of precipitation isotope variability across the tropical Pacific in observations and SWING2 model simulations

Jessica L. Conroy,[1] Kim M. Cobb,[1] and David Noone[2]

Received 11 December 2012; revised 10 April 2013; accepted 11 April 2013; published 13 June 2013.

[1] Probing the dynamics of the Earth's hydrologic cycle benefits from the use of isotope-equipped global climate models. However, isotope model simulations are not often compared together, along with existing observations, to assess the distribution of simulated stable isotope variability. Here we evaluate the spatial and temporal patterns of tropical Pacific precipitation isotope variability in global climate models from the second Stable Water Isotope Intercomparison Group experiment and in observations. The tropical Pacific is home to many isotope-based proxies of paleoclimatic change, and as such is an important target for such model-data comparisons. We find spatial and temporal examples of precipitation-isotope mismatches, highlighting that factors beyond the amount effect influence precipitation isotope variability across the tropical Pacific. The models that best capture mean annual precipitation in the tropical Pacific are not necessarily the models that best simulate the mean annual stable isotopic composition of precipitation. Nudging with reanalysis winds has a small effect on precipitation $\delta^{18}O$ values. Model performance and the strength of the relationship between precipitation and precipitation $\delta^{18}O$ values varies between the western, central, and eastern equatorial Pacific. In the majority of the simulations, western equatorial Pacific $\delta^{18}O$ values are correlated with large-scale, but not local precipitation, whereas in the central and eastern equatorial Pacific, $\delta^{18}O$ values are correlated most strongly with regional precipitation. This comparison provides a cautionary note on using results from a single model to assist in interpretation of paleoclimate proxy records.

Citation: Conroy, J. L., K. M. Cobb, and D. Noone (2013), Comparison of precipitation isotope variability across the tropical Pacific in observations and SWING2 model simulations, *J. Geophys. Res. Atmos.*, *118*, 5867–5892, doi:10.1002/jgrd.50412.

1. Introduction

[2] The stable isotope ratios of precipitation (D/H and $^{18}O/^{16}O$) serve as important tracers of the hydrologic cycle due to the atomic mass and vapor pressure differences that drive isotopic fractionation during water phase changes. This fractionation produces stable isotopic signatures that correlate to climate variables such as temperature, precipitation amount, and air mass history [*Dansgaard*, 1964; *Rozanski et al*., 1993; *Gat*, 1996]. The origin of these climate-isotope correlations lies in the dependence of both the stable isotopic composition of precipitation and the climate variables on underlying atmospheric physics. These relationships are of special significance in paleoclimatic research, as they underpin many of the interpretations of past climate change derived from water isotope proxies such as ice cores, speleothems, trees, corals, and sediment records [e.g., *Thompson et al*., 2006; *Partin et al*., 2007; *Anchukaitis et al*., 2008; *Tierney et al*., 2010]. Thus, it is of utmost importance that the climate drivers of precipitation isotope variability are well defined in the present day. To that end, isotope-equipped global climate models (GCMs) can be used to enhance our understanding of the physical links between climate and water isotopes. Simulations of stable isotope ratios are particularly important given the limited spatial and temporal coverage of water isotope observations in many regions of the world. Furthermore, as we turn to isotopic proxies of past water cycle variability to understand the full range of hydroclimatic variability in the Earth system, GCM simulations that include water isotope tracers can help to identify past climatic controls on water isotope variability, which may vary during periods with different external forcing factors, such as the Last Glacial Maximum and the mid-Holocene.

[3] In the tropical Pacific, large changes in both regional and global hydroclimate are captured in numerous water isotope-based climate proxies that are used to study past changes in tropical Pacific climate, including the El Niño-Southern Oscillation (ENSO). Such records are particularly valuable in this region, where the instrumental record of climate is sparse

Additional supporting information may be found in the online version of this article.

[1]School of Earth and Atmospheric Sciences, Georgia Institute of Technology, Atlanta, Georgia, USA.

[2]Department of Atmospheric and Oceanic Sciences, and Cooperative Institute for Research in Environmental Sciences, University of Colorado, Boulder, Colorado, USA.

Corresponding author: J. L. Conroy, School of Earth and Atmospheric Sciences, Georgia Institute of Technology, Atlanta, GA, USA. (jconroy8@mail.gatech.edu)

2169-897X/13/10.1002/jgrd.50412

in space and time prior to the mid-20th century. Direct observations of tropical Pacific precipitation isotopes, while rare, indicate that the primary control on tropical precipitation isotope variability is precipitation amount, particularly on a mean annual and seasonal basis [*Dansgaard*, 1964; *Rozanski et al*., 1993; *Araguas-Araguas et al*., 1998]. However, water isotope variability on interannual to decadal time scales is poorly constrained by the available observations, hampering the interpretation of isotope-based records of tropical Pacific paleoclimate. Thus, model simulations of isotopic variability are key to elucidating the full range climate controls on water isotopes in this region on seasonal and longer time scales, controls which may include changing source regions, shifting vapor trajectories, large-scale convergence and divergence, evaporation, and interaction with subcloud vapor [*Cole et al*., 1999; *Cobb et al*., 2007; *Lee et al*., 2007; *Kurita et al*., 2009; *Berkelhammer et al*., 2012; *Moerman et al*., 2013].

[4] Following the first simulation of water isotopes in a GCM [*Joussaume et al*., 1984], there have been numerous simulations of water isotope variability in many different atmospheric, and more recently, coupled ocean-atmosphere GCMs [e.g., *Hoffmann et al*., 1998; *Cole et al*., 1999; *Mathieu et al*., 2002; *Noone and Simmonds*, 2002; *Vuille et al*., 2003; *Brown et al*., 2006; *Schmidt et al*., 2006; *Lee et al*., 2007; *Schmidt et al*., 2007; *LeGrande and Schmidt*, 2009; *Sime et al*., 2009; *Tindall et al*., 2009; *Risi et al*., 2010; *Kurita et al*., 2011]. These model simulations are used to investigate the hydrologic cycle in both the past and present day, but there are few published comparisons of water isotope simulations from different GCMs [*Jouzel et al*., 2000; *Vuille et al*., 2003; *Risi et al*., 2012]. For practical reasons, many diagnostic studies are based on analysis of isotope output from one model. As such, there are few intercomparisons of model isotope output with available observational data across a range of frequencies. To make the best use of model isotope outputs in paleodata-model intercomparison studies, robust metrics for comparing model output with instrumental isotope data must be developed.

[5] The physical processes that govern isotopic fractionation are well known, but individual model parameterizations of fractionation processes are intimately coupled to the models' precipitation schema, which differ appreciably [*Dai*, 2006; *Lee et al*., 2009]. Model treatment of kinetic fractionation or rain-vapor equilibration leads to further differences between simulations [*Stewart*, 1975; *Lee and Fung*, 2007]. An intercomparison of precipitation isotope output from GCMs, coupled with a rigorous comparison to existing observational data, can be useful in quantifying and diagnosing model biases. Furthermore, assessing the degree of intermodel spread with regard to isotopic variability at a particular site can guide the choice of specific models for the investigation of regionally-specific water isotope variability that might be captured in a given set of water isotope-based paleoclimate reconstructions.

[6] Here we present a survey of twelve different model simulations of modern-day tropical Pacific climate that include water isotopes, and compare their output to observations from across the tropical Pacific. Our goal is to identify the most important climate processes governing water isotope variability across the tropical Pacific, to inform the interpretations of water isotope-based proxies in the region. Therefore, we primarily focus on the $\delta^{18}O$ value of precipitation (henceforth $\delta^{18}O_p$) and precipitation amount in each model simulation. We investigate the relationship between $\delta^{18}O_p$ and precipitation variability across the tropical Pacific basin (25°S–25°N, 110°E–75°E) in each simulation on mean annual, seasonal and interannual time scales. We also quantify the strength of the tropical Pacific amount effect, the strong negative correlation between precipitation amount and $\delta^{18}O_p$ [*Dansgaard*, 1964]. In the second part of the paper, we assess $\delta^{18}O_p$ variability and its relationship to local and large-scale precipitation variability at three sites (Palau, Kiritimati, and Galápagos) where well-known water isotope reconstructions have been generated. The motivation for this individual point-based analysis is to explore, to the extent possible, what individual proxy records of $\delta^{18}O_p$ can tell us about large-scale hydroclimatic variability across the tropical Pacific basin.

2. Models and Methods

[7] We evaluate 12 simulations from eight atmosphere-only GCMs and one coupled ocean-atmosphere GCM (see Table 1 for model information) that participated in the second Stable Water Isotope Intercomparison Group (SWING2, http://people.su.se/~cstur/SWING2) [*Sturm et al*., 2010]. All atmosphere GCM simulations were forced with observed sea surface temperature (SST). Precipitation and the stable isotopic composition of total precipitation (the sum of large-scale and convective precipitation for each grid), reported as $\delta^{18}O$ and δD, are assessed in all the simulations. In the case of the GENESIS3 simulation, model $\delta^{18}O_p$ values were 6‰ too low globally relative to observations and the results reported in *Mathieu et al*. [2002]. We corrected for this offset by adding 6‰ to each individual $\delta^{18}O_p$ value in the data set. Of the twelve model simulations, four were nudged with reanalysis winds using methods similar to those described by [*Noone*, 2006] and [*Yoshimura et al*., 2008]. Three of the four nudged simulations also have "free" simulations archived in the SWING2 database, which allows evaluation of the impact of nudging on tropical Pacific precipitation and $\delta^{18}O_p$. The analysis is based on monthly data from 1980 to 1999, to compare the common period across all the archived model simulations. For the one coupled model simulation in the SWING2 archive, the Hadley Centre Coupled Model, version 3 (HadCM3), the last 20 years of the simulation are considered. Although HadCM3 is forced by top of the atmosphere radiative forcing rather than observed SST, we consider it along with the atmosphere-only simulations as it represents an equally valid realization of the global hydrological cycle. However, without being constrained by observed SST or reanalysis meteorology, the HadCM3 result is distinctive. Individual gridded values of $\delta^{18}O_p$ and precipitation are compared with gridded Global Precipitation Climatology Project (GPCP) 2.2 precipitation data [*Adler et al*., 2003], and monthly station values of $\delta^{18}O_p$ from the Global Network of Isotopes in Precipitation (GNIP) and the Japan Agency for Marine-Earth Science and Technology (JAMSTEC) databases [*IAEA/WMO*, 2006; *Kurita et al*., 2009]. To investigate mean annual and seasonal variability, only stations from 25°S to 25°N, 110°E to 75°W in the GNIP and JAMSTEC database with a complete year of both $\delta^{18}O_p$ and precipitation values are considered. For investigation of ENSO and the temporal amount effect, only those stations with at least sixty months of observations are considered (Table 2). During investigation of the spatial amount effect in observations, only near ocean observations are evaluated, as the amount effect is absent or damped in continental and

Table 1. Model Name, Key Reference, Resolution, and Simulations Considered in This Publication

Model	Key Reference	Simulations	Grid Resolution
CAM2	*Lee et al.* [2007]	Free	2.8°×2.8°
ECHAM4	*Hoffmann et al.* [1998]	Nudged with ECMWF	2.8°×2.8°
MIROC	*Kurita et al.* [2011]	Free	2.8°×2.8°
GENESIS3	*Mathieu et al.* [2002]	Free	3.75°×3.75°
LMDZ4	*Risi et al.* [2010]	Free and nudged with ECMWF	2.5°×3.75°
GISS	*Schmidt et al.* [2007]	Free and nudged with NCEP	2°×2.5°
GSM	*Yoshimura et al.* [2008]	Free and nudged with NCEP	1.9°×1.9°
HadAM3	*Sime et al.* [2009]	Free	2.5°×3.75°
HadCM3	*Tindall et al.* [2009]	Free (no SST forcing)	2.5°×3.75°

high-elevation regions, which bias the observational record from the tropical Pacific (Table 1). In comparing station $\delta^{18}O_p$ values to simulated $\delta^{18}O_p$ values, it is important to note that a single grid-box comprises a much larger area than an individual station.

3. Intermodel Comparisons

3.1. Mean Annual Isotope Variability and the Amount Effect

[8] In model simulations, the amount effect is often considered the primary driver of $\delta^{18}O_p$ variability in the tropical Pacific on a mean annual basis [*Noone and Simmonds*, 2002; *Brown et al.*, 2006; *Lee et al.*, 2007; *Tindall et al.*, 2009]. Thus, lower mean annual $\delta^{18}O_p$ values occur in regions of greater mean annual precipitation. All the models simulate a characteristic mean annual spatial pattern of tropical Pacific isotope variability that includes higher $\delta^{18}O_p$ values in dry regions of the cold tongue and subtropical gyres and lower $\delta^{18}O_p$ values in the wetter regions of the west Pacific warm pool, parts of the Intertropical Convergence Zone (ITCZ) and the South Pacific Convergence Zone (SPCZ) (Figure 1).

[9] In Figure 1, the existing observational data are plotted in the uppermost row of each column for comparison to the simulations. Although the data are sparse, simulated mean annual patterns of $\delta^{18}O_p$ resemble observations, with lower $\delta^{18}O_p$ in the wetter western Pacific and higher $\delta^{18}O_p$ in drier central and eastern Pacific, and in subtropical gyre regions. A previous analysis of the global GNIP data set also revealed higher $\delta^{18}O_p$ in subtropical regions and lower $\delta^{18}O_p$ within the global ITCZ [*Feng et al.*, 2009]. In most simulations, $\delta^{18}O_p$ is also lower over higher elevation continental regions, such as the Andes, in accordance with the altitude effect. Most models also simulate mean annual patterns of precipitation similar to satellite precipitation observations, but one common discrepancy is that precipitation magnitude in the ITCZ and SPCZ is too high in many of the model simulations. The largest offset from observed precipitation and $\delta^{18}O_p$ is found in the coupled ocean-atmosphere HadCM3. HadCM3 has a double ITCZ, a common problem in coupled model simulations [*Lin*, 2007], leading to a "U"-shaped area of increased precipitation and lower $\delta^{18}O_p$ values stretching from the western Pacific, along 20°S in the central Pacific and up to 10°N–20°N in the eastern Pacific.

[10] In all the model simulations, mean annual $\delta^{18}O_p$ patterns are negatively correlated with mean annual precipitation patterns, with spatial correlation coefficients ranging from –0.42 to –0.75 (Figure 1). This distribution contains the spatial correlation coefficient of –0.48 ($N = 31$) calculated from near-ocean sites in the observational data set. The NCAR Community Atmosphere Model (CAM2) produces the weakest spatial amount effect ($r = –0.42$), most similar to observations, whereas most of the other model simulations produce spatial amount effects that are larger than observed. Unlike other models, CAM2 includes an isotope equilibrium parameterization that accounts for drop size, humidity, rain rate, and temperature, which may play a role in reducing the strength of the amount effect in this model [*Lee and Fung*, 2007]. This suggests that accounting for variability in rain interaction with subcloud vapor may act to reduce the cloud signal in precipitation, although this cannot be confirmed with the existing model output. Overestimation of the amount effect in other simulations may be partly due to simplified equilibration parameterizations, such as the 95% equilibration for stratiform rain and 45% equilibration for convective rain used in many of the simulations [*Hoffmann et al.*, 1998].

[11] Spatial correlation coefficients provide insight into the range of modeled amount effects, but oversimplify the relationship between $\delta^{18}O_p$ and precipitation in some regions. Examples of more complex relationships between $\delta^{18}O_p$ and precipitation occur in the Goddard Institute for Space Studies General Circulation Model (GISS) simulations, which show spatial scatter in precipitation values in the western tropical Pacific and Central America, yet isotopic values in these areas that are more spatially coherent. This precipitation-isotope mismatch is an indication that local precipitation amount is not the sole driving force behind $\delta^{18}O_p$ variability in precipitation in these regions. A weak relationship between monthly $\delta^{18}O_p$ and local rainfall amount in the western tropical Pacific has also been noted in observational studies [*Cobb et al.*, 2007; *Kurita et al.*, 2009; *Moerman et al.*, 2013]. Additionally, sharp zonal and meridional gradients exist in the tropical Pacific precipitation fields plotted in Figure 1, yet in some simulations $\delta^{18}O_p$ values are more diffuse across these boundaries. For example, the ITCZ is strongly defined in the mean annual precipitation fields in the CAM2, Model for Interdisciplinary Research on Climate (MIROC), Laboratoire de Météorologie Dynamique-Zoom (LMDZ), LMDZ nudged, GSM, and Global Spectral Model (GSM) nudged simulations, but in these simulations the ITCZ is not as prominently expressed in $\delta^{18}O_p$ values.

[12] The lack of a strongly defined isotopic ITCZ in half of the simulations could be due to similar rates of rain equilibration with ambient vapor both in and outside of the ITCZ [*Jouzel*, 1986]. Equilibration during rainfall could also occur with boundary layer vapor with similar isotopic values both inside and outside the ITCZ. For example, simulated vapor isotopes in CAM2 are nearly uniform across the tropics, due to the greater importance of evaporative surface fluxes relative to cloud processes, despite large changes in P-E [*Lee et al.*, 2007]. These types of precipitation-isotope mismatches highlight the potential importance of understanding regional differences in the individual contributors to the amount effect, which include the re-evaporation of falling rain, diffusive exchanges between raindrops and vapor in unsaturated downdrafts, the recycling of the depleted vapor from downdrafts back into the convective system [*Risi et al.*, 2008, 2008b], rain

Table 2. List of Stations With Precipitation Stable Isotope Data Used in This Analysis

Site Name	Lat	Lon	Elevation (m)	N $\delta^{18}O_p$	Years Sampled	Source
Albania	3.44	–76.01	3000	24	2003–2004	GNIP
Alice Springs	–23.8	133.88	546	155	1962–1987	GNIP
Alluriquin	–0.32	–78.98	1378	25	1992–1996	GNIP
Amaluza	–2.61	–78.57	2378	27	1992–1994	GNIP
Apia	**–13.8**	**–171.78**	**2**	**111**	**1962–1977**	**GNIP**
Bacon Manito (averaged)	13.04	123.94	472	35	1990–1998	GNIP
Bellavista	**–0.42**	**–90.22**	**194**	**143**	**1995–2008**	**GNIP**
Canton Island	**–2.77**	**–171.72**	**2**	**47**	**1962–1967**	**GNIP**
Christmas Island	**1.98**	**–157.46**	**3**	**23**	**1962–1964**	**GNIP**
Corozal	9.34	–75.29	175	66	2002–2007	GNIP
Cuenca	–2.89	–79	2536	24	1992–1996	GNIP
Darwin	**–12.43**	**130.87**	**26**	**241**	**1962–2000**	**GNIP**
Dilman Quezon City	**14.64**	**121.04**	**42**	**92**	**2000–2008**	**GNIP**
El Jaral	14.94	–88.02	652	26	2007–2009	GNIP
Esmeraldas	**0.95**	**–79.65**	**50**	**18**	**1992–1996**	**GNIP**
Guangzhou	**23.13**	**113.32**	**7**	**30**	**1986–1989**	**GNIP**
Haikou	**20.03**	**110.35**	**15**	**59**	**1988–2000**	**GNIP**
Havana	**23.17**	**–82.33**	**40**	**12**	**1989–1991**	**GNIP**
Havana (CPHR)	**23.05**	**–82.22**	**137**	**87**	**2002–2009**	**GNIP**
Hilo	**19.72**	**–155.07**	**9**	**87**	**1960–1974**	**GNIP**
Hong Kong	**22.32**	**114.17**	**66**	**442**	**1961–2008**	**GNIP**
Howard Air Force Base	**8.92**	**–79.6**	**13**	**231**	**1968–1997**	**GNIP**
Izobamba	–0.37	–78.55	3492	243	1968–2008	GNIP
Jayapura	**–2.53**	**140.72**	**3**	**309**	**1961–1991**	**GNIP**
Johnston Island	**16.73**	**–169.52**	**2**	**92**	**1962–1976**	**GNIP**
La Concordia	–0.22	–79.63	150	27	1992–1996	GNIP
Lago Agrio	0.08	–76.87	369	24	1992–1996	GNIP
Leyte (averaged)	11.14	124.65	567	12	1997–1998	GNIP
Machala	**3.27**	**79.17**	**3**	**20**	**1992–1996**	**GNIP**
Madang	**–5.22**	**145.8**	**4**	**125**	**1968–1982**	**GNIP**
Makassar	**–5.07**	**119.55**	**14**	**43**	**2002–2006**	**JAMSTEC**
Manado	**1.53**	**124.92**	**80**	**45**	**2002–2006**	**JAMSTEC**
Manila	**14.52**	**121**	**14**	**48**	**1961–1976**	**GNIP**
Marcapomacocha	–11.4	–76.33	4477	34	2006–2009	GNIP
Mendez	–2.72	–78.32	1826	23	1992–1994	GNIP
Mt Apo (averaged)	7.01	125.23	1354	12	1993–1998	GNIP
Palau	**7**	**134.27**	**2**	**48**	**2002–2006**	**JAMSTEC**
Panama Universidad	**8.98**	**–79.53**	**5**	**28**	**2002–2006**	**GNIP**
Papallacta	–0.38	–78.14	3692	21	1992–1994	GNIP
Quito-Inamhi	–0.17	–78.48	2789	106	1997–2009	GNIP
Rarotonga	**–21.2**	**–159.8**	**6**	**132**	**1979–1991**	**GNIP**
Sacamento	10.108	–84.116	2260	21	1990–2004	GNIP
San Salvador	13.7	–89.12	615	98	1968–1984	GNIP
Santa Maria	10.77	–85.32	825	26	1990–1998	GNIP
Southern Negros (averaged)	9.29	123.18	738	21	1991–1998	GNIP
Taguac	**13.55**	**144.83**	**110**	**112**	**1961–1977**	**GNIP**
Tarawa	**1.35**	**172.92**	**4**	**17**	**1990–1991**	**GNIP**
Tawau (averaged)	**4.37**	**117.91**	**286**	**12**	**2007–2008**	**GNIP**
Truk	**7.47**	**151.85**	**2**	**93**	**1968–1977**	**GNIP**
Uzhcurrumi	–3.33	–79.61	300	33	1992–1996	GNIP
Veracruz	**19.2**	**–96.13**	**16**	**172**	**1962–1988**	**GNIP**
Wake Island	**19.28**	**166.65**	**3**	**151**	**1962–1976**	**GNIP**
Yap	**9.49**	**138.09**	**23**	**99**	**1968–1976**	**GNIP**

Bold sites are those that are near-ocean and low elevation, which are assessed in the spatial amount effect scatter plots of Figures 1, 4–6.

drop size, temperature, and subcloud relative humidity [*Lee and Fung*, 2007]. Additionally, vapor source region, moisture transport, and lateral mixing likely also play a key role in determining $\delta^{18}O_p$ at a given location.

[13] Given the strong zonal differences and interannual variability in mean tropical Pacific climate, particularly with regard to many of the factors influencing the amount effect, it is likely the strength of the temporal amount effect varies across the tropical Pacific basin. Figure 2 shows the correlation coefficients between $\delta^{18}O_p$ and precipitation time series for all months from 1980–1999 for each individual model grid cell. There is a strong, negative temporal relationship between $\delta^{18}O_p$ and precipitation across much of the tropical Pacific in all simulations and in observations. However, the strength of the precipitation-$\delta^{18}O_p$ relationship varies between the eastern, central, and western Pacific. Drier regions such as the eastern tropical Pacific, especially south of the equator, consistently do not show a strong temporal amount effect, as previously observed in other simulations [*Hoffmann et al*., 1998; *Noone and Simmonds*, 2002; *Vuille et al*., 2003]. Across all the simulations, the temporal amount effect is strongest in the central equatorial Pacific and in Northern Hemisphere subtropical regions. The temporal amount effect is also weaker in the western equatorial

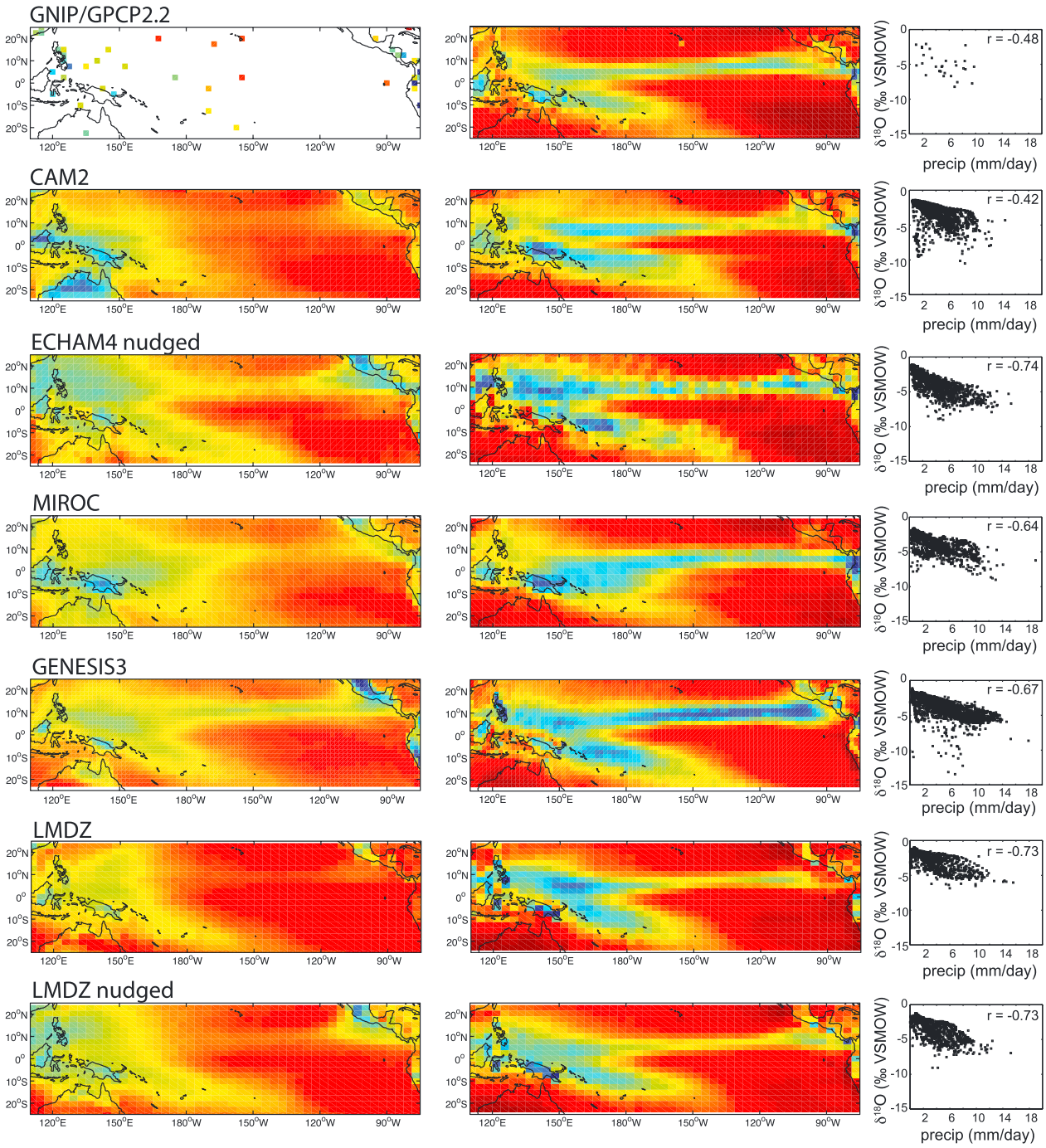

Figure 1. Mean annual, amount weighted $\delta^{18}O_p$ values (left column) and mean annual precipitation values (middle column) for the tropical Pacific region from existing observations and model simulations. Scatterplots of gridded mean annual $\delta^{18}O_p$ and precipitation values are shown in right column, along with linear correlation coefficients. For scatterplot of observations, we only assess station precipitation and $\delta^{18}O_p$ at low elevation, near-ocean sites. We do not compare observed $\delta^{18}O_p$ data and GPCP2.2 observations, as much of the isotope data predate GPCP2.2. Note colorbars are flipped between $\delta^{18}O_p$ and precipitation here and in subsequent figures, so wetter conditions/lower $\delta^{18}O_p$ are blue, and drier conditions/higher $\delta^{18}O_p$ are red.

Pacific, with the relationship usually weakening west of the dateline in many simulations. Using Spearman rank coefficients to allow for non-normal data distributions in some arid regions produced comparable results for all the model simulations as those plotted in Figure 2.

[14] The scatterplots in Figure 1 indicate the spatial amount effect is much stronger in most simulations compared to observations. Broadly, all models also simulate temporal correlation coefficients between $\delta^{18}O_p$ and precipitation that are also stronger than observed correlation

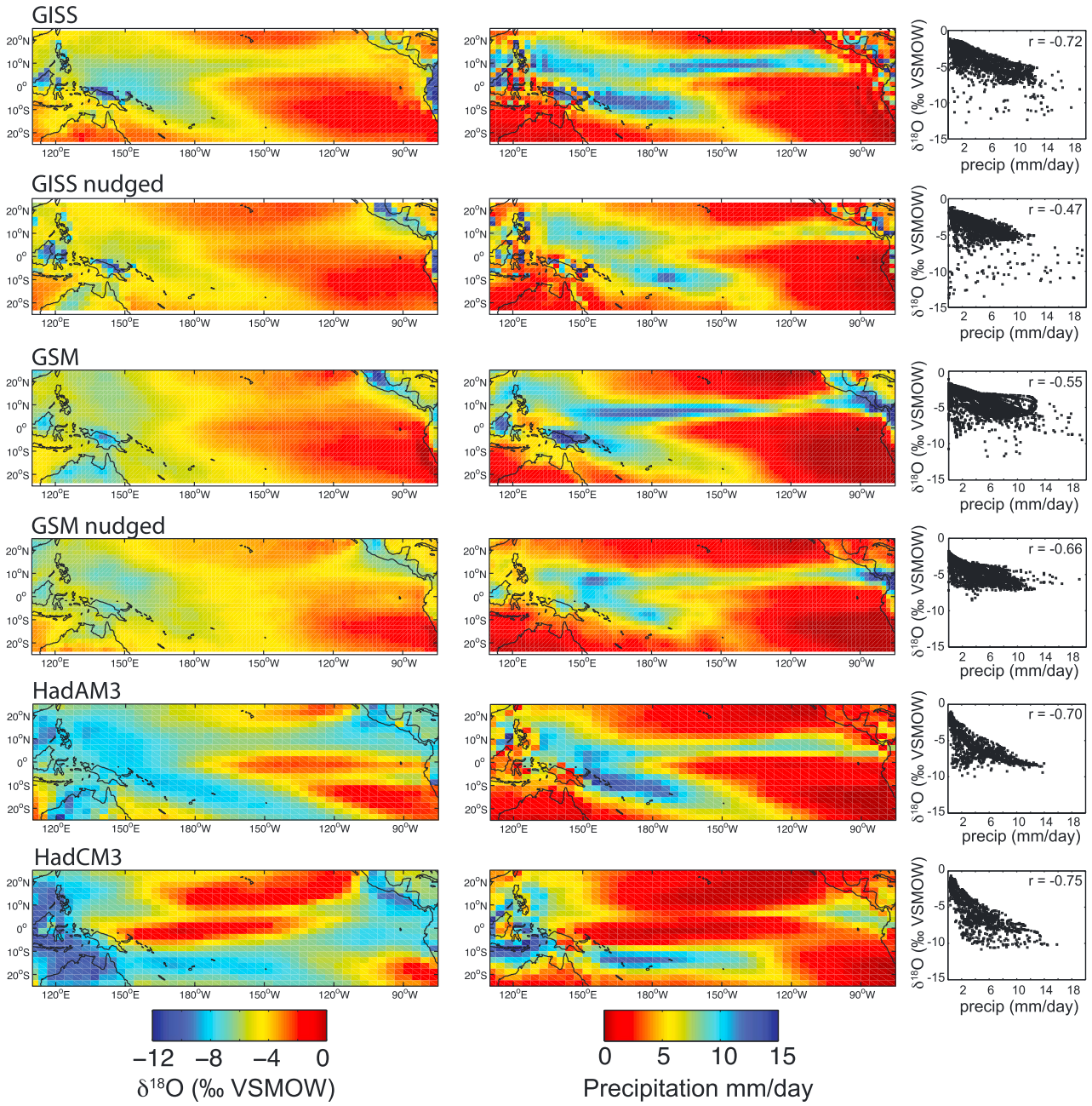

Figure 1. (continued)

coefficients. Previous studies have also noted this inflation of amount effect correlation coefficients in model simulations [*Hoffmann et al.*, 1998; *Cole et al.*, 1999; *Mathieu et al.*, 2002; *Lee et al.*, 2007]. In Figure 2, the observed correlation coefficients between monthly station measurements of $\delta^{18}O_p$ and precipitation range from –0.25 to –0.71. In the SWING2 model simulations, LMDZ, LMDZ nudged, Hadley Centre Atmospheric Model version 3 (HadAM3), and HadCM3 have the strongest $\delta^{18}O_p$–precipitation correlation coefficients, with values between –1.0 and –0.9 in some regions. The CAM2, GISS, and GISS nudged simulations contain smaller correlation coefficients, especially in the western and eastern tropical Pacific. There are several possible reasons for these model differences in the strength of the amount effect. A stronger simulated amount effect has been hypothesized to be due to insufficient observed data over the open ocean, hindering validation of the isotopic simulations [*Lee et al.*, 2007]. Model deficiencies could include convective precipitation height that is too high [*Hoffmann et al.*, 1998], or, as we observe that one of the simulations with the weakest temporal amount effect is CAM2, it could be due to insufficient representation of raindrop interaction with subcloud vapor, which would act to mute the cloud process signal in the resulting precipitation.

3.2. Taylor Diagrams of Mean Annual $\delta^{18}O_p$ and Precipitation

[15] Taylor diagrams for both mean annual precipitation and mean annual, amount-weighted $\delta^{18}O_p$ values reveal

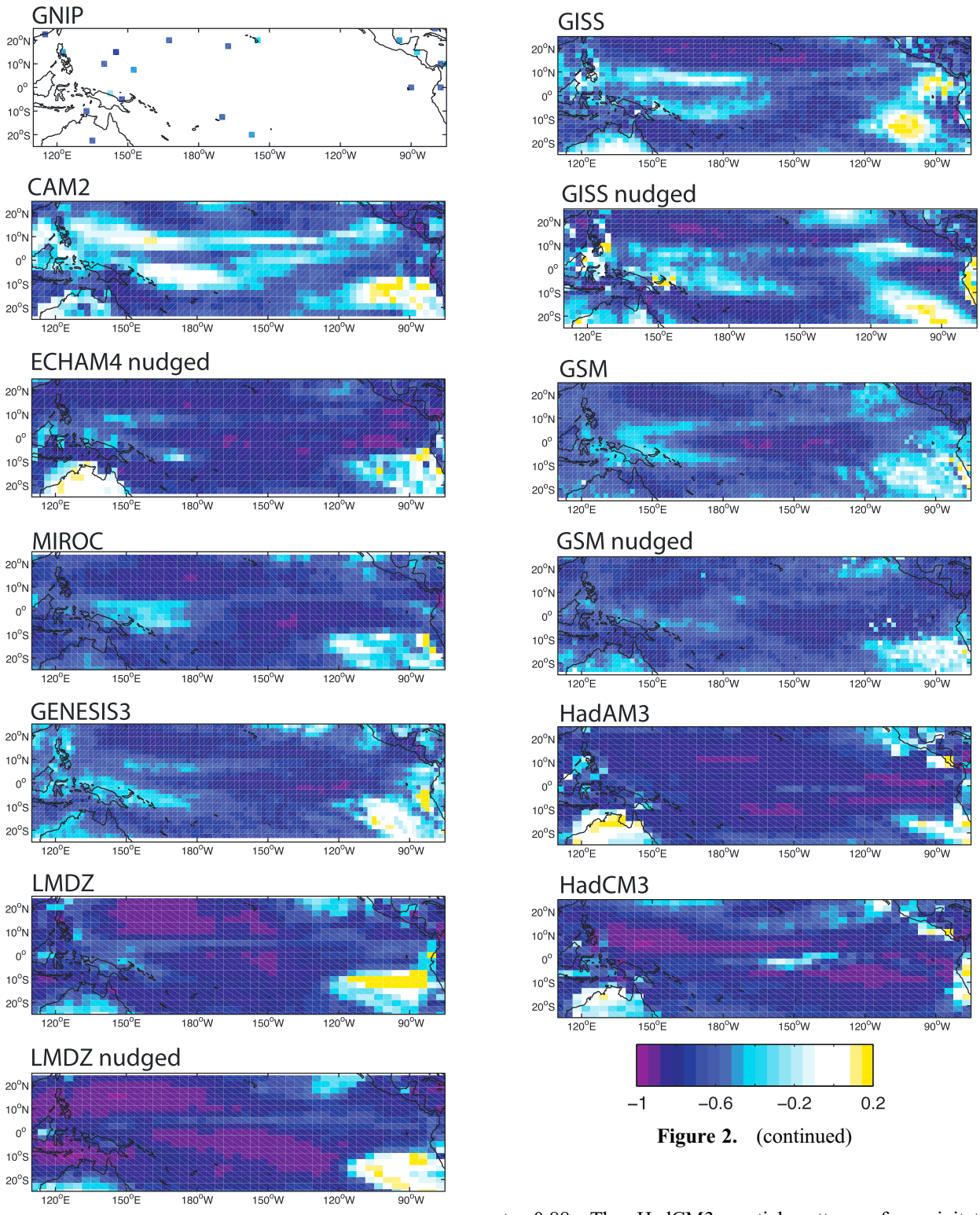

Figure 2. (continued)

Figure 2. Correlation coefficients of monthly $\delta^{18}O_p$ values and monthly precipitation values for each grid. For observed $\delta^{18}O_p$, we only plot stations with more than sixty months of data.

intermodel differences in mean annual $\delta^{18}O_p$ and precipitation and their similarity to observations (Figure 3). Most models accurately simulate the spatial pattern of tropical Pacific precipitation, with correlation coefficients between simulated and observed GPCP2.2 precipitation ranging from 0.75 to 0.88. The HadCM3 spatial pattern of precipitation diverges most from observations ($r = 0.44$), as apparent in Figure 1. The standard deviation of modeled precipitation fields ranges from 2.5–3.5 mm/d, greater than the standard deviation in GPCP2.2 observations, although model standard deviations approach the mean CPC Merged Analysis of Precipitation standard deviation for tropical Pacific precipitation [*Xie and Arkin*, 1997]. All the simulations have root mean square difference (RMSD) values between 1–2 mm/d, with the exception of HadCM3, which has a RMSD of

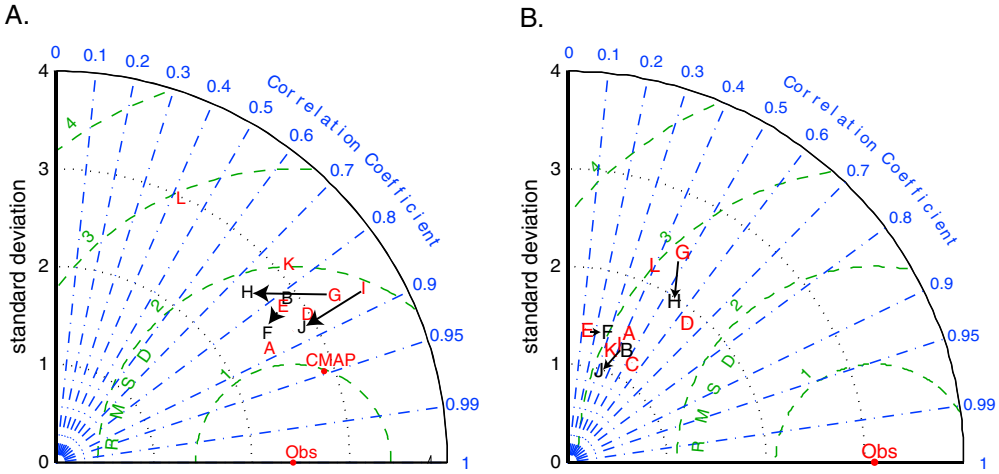

Figure 3. Taylor diagrams of (A) mean annual precipitation and (B) mean annual amount weighted $\delta^{18}O_p$ values for the tropical Pacific from existing observations and model simulations. Black letters indicate nudged model simulations, arrows indicate change from "free" model simulation to model nudged with reanalysis winds. Simulations denoted by letters: A: CAM2 B: ECHAM4 nudged C: MIROC D: GENESIS3 E: LMDZ F: LMDZ nudged G: GISS H: GISS nudged I: GSM J: GSM nudged K: HadAM3 L: HadCM3 (a coupled ocean-atmosphere model). "Obs" for rain indicates GPCP2.2 data set and monthly station $\delta^{18}O_p$ values for isotopes.

nearly 3 mm/d. Figure 3a indicates the CAM2, ECMWF Hamburg Model (ECHAM4) nudged, MIROC, GENESIS3, LMDZ, and LMDZ nudged simulations produce mean annual precipitation values that are closest to observed precipitation statistics.

[16] Although mean annual spatial patterns of $\delta^{18}O_p$ are relatively coherent with mean annual precipitation patterns in the tropical Pacific, and several GCMs perform well with respect to precipitation, there is more spread in model $\delta^{18}O_p$ performance (Figure 3b). Correlation coefficients between modeled and observed mean annual weighted $\delta^{18}O_p$ range from 0.12 to 0.65, much lower values compared to the correlation coefficients between observed and modeled precipitation. This is at least partly due to the problems of comparing localized station data to the large areas that comprise model grid cells, as well as the shorter length and the varying time periods of the observational $\delta^{18}O_p$ data. GENESIS3 best captures the spatial pattern of observed $\delta^{18}O_p$ variability ($r = 0.65$), but underestimates the observed standard deviation in $\delta^{18}O_p$. Model $\delta^{18}O_p$ standard deviations range from 1.0–2.4‰, with GISS free and HadCM3 producing the standard deviations that are closest to the observed standard deviation of 3.1‰. RMSDs between simulations and observations range between 2.4 and 3.2‰.

[17] Although the greater spread in modeled $\delta^{18}O_p$ versus precipitation statistics could be a result of insufficient observed $\delta^{18}O_p$ data, the differences in model performance for $\delta^{18}O_p$ versus precipitation do suggest that model-observed differences in $\delta^{18}O_p$ are not just a result of incorrect precipitation simulations. The greater discrepancies in $\delta^{18}O_p$ could be due to inadequate incorporation of isotopic physics into bulk-scale cloud parameterizations, especially the treatment of fractionation in convective clouds, or incorrect simulations of nonhydrologic variables, like wind direction, that may play a crucial role in determining source regions. Small-scale, high frequency hydrologic variability that is not represented in GCMs, and may lead to organized structure, such as the Madden-Julian Oscillation, may also play a key role in determining mean monthly $\delta^{18}O_p$ values. Incorrect representation of this variability may contribute to the modeled and observed $\delta^{18}O_p$ differences [*Kurita et al.*, 2011; *Berkelhammer et al.*, 2012].

3.3. Seasonal and Interannual Isotope Variability

[18] Seasonality in precipitation and $\delta^{18}O_p$ values is depicted in Figure 4 as the difference between mean June-July-August (JJA) precipitation and $\delta^{18}O_p$ values and December-January-February (DJF) precipitation and $\delta^{18}O_p$ values. The seasonal patterns of precipitation and $\delta^{18}O_p$ in most model simulations are similar to observations. Both increased precipitation and lower $\delta^{18}O_p$ values are present north of the equator in JJA, as the ITCZ maintains a northerly position. Precipitation increases and $\delta^{18}O_p$ values decrease in DJF south of the equator, especially within the SPCZ. In the near ocean observations, the seasonal amount effect is stronger compared to mean annual spatial amount effect ($r = -0.73$, $n = 31$). We also find that the seasonal spatial amount effect is stronger than the mean annual spatial amount effect in 9 of the 12 simulations, with spatial correlation coefficients ranging from –0.55 to –0.92 (Figure 4). However, isotopic seasonality is strongest near the continents, and weak in equatorial, open-ocean regions, despite strong precipitation seasonality near the equator in some simulations. This particular pattern of seasonal isotopic differences is manifested most strongly in those simulations with a weak isotopic expression of the mean ITCZ. Simulated $\delta^{18}O_p$ seasonality is also weak in the northern subtropical gyre and in the southeastern tropical Pacific in all the simulations, with the exception of HadCM3.

[19] Interannual variability in $\delta^{18}O_p$ is manifested strongly across the tropical Pacific in model simulations [*Hoffmann et al.*, 1998; *Cole et al.*, 1999; *Noone and Simmonds*, 2002; *Vuille et al.*, 2003; *Brown et al.*, 2006; *Tindall et al.*, 2009]

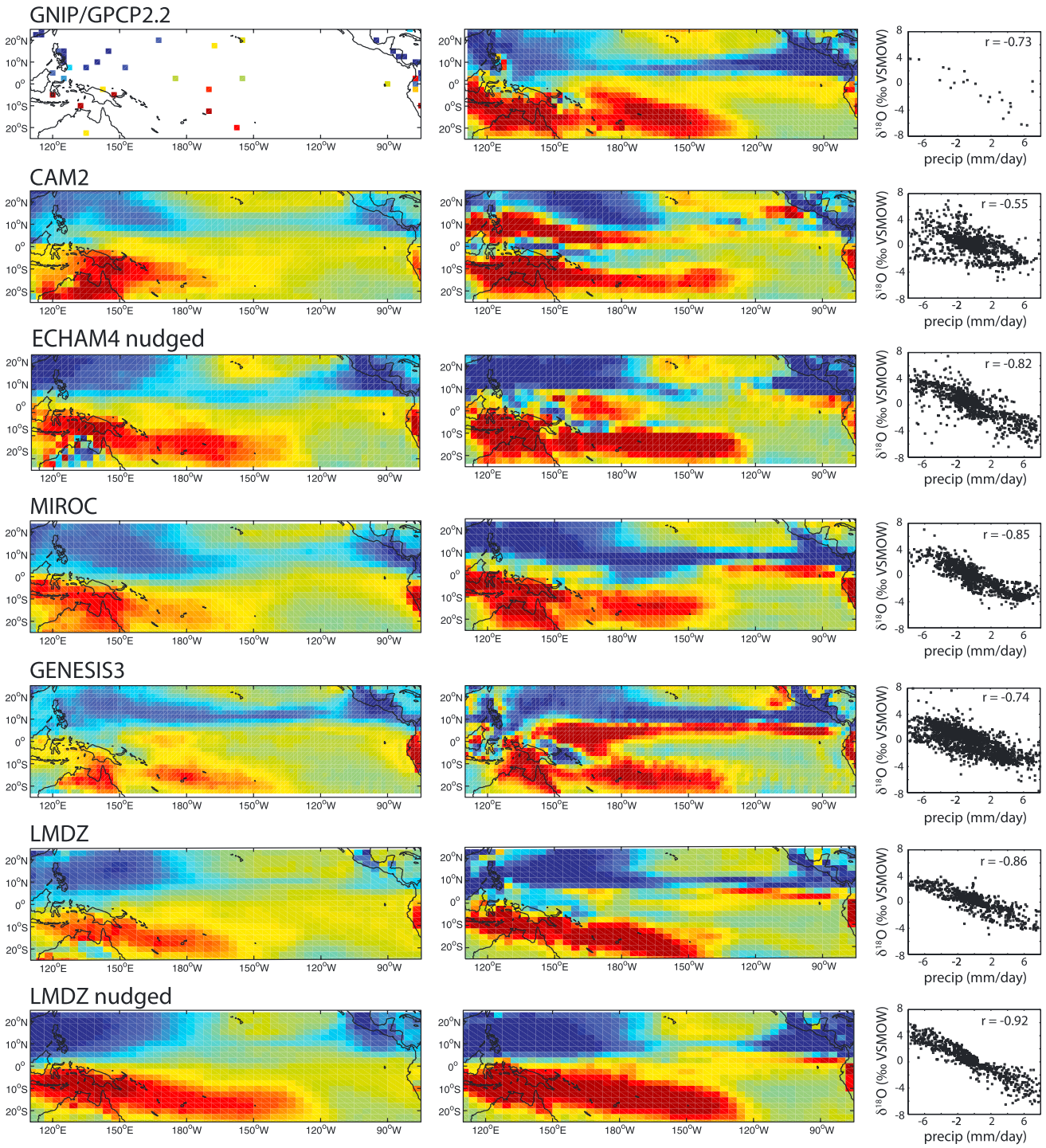

Figure 4. Mean, amount weighted $\delta^{18}O_p$ (left column) and precipitation values (right column) for boreal summer (JJA) minus boreal winter (DJF) across the tropical Pacific from existing observations and model simulations. Scatterplots of gridded JJA-DJF $\delta^{18}O_p$ and precipitation values are shown in right column, along with linear correlation coefficients. For scatterplot of observations, we only assess low elevation, near-ocean stations.

as ENSO influences precipitation amount, and other factors, like atmospheric circulation patterns, that also impart an influence on $\delta^{18}O_p$ [*Vuille et al.*, 2003]. The interannual $\delta^{18}O_p$ and precipitation signature in the tropical Pacific within the SWING2 model simulations is shown by a composite of average $\delta^{18}O_p$ and precipitation values during El Niño months minus the long-term mean and average $\delta^{18}O_p$ and precipitation during La Niña months minus the long-term mean (Figures 5 and 6). El Niño months are defined as months where surface temperature anomalies in the NIÑO3.4 region (5°S–5°N, 170°W–120°W) are greater than 0.5°C (less than 0.5°C for La Niña months). For the observational data, we used ERSST v3b NIÑO3.4 Index values [*Smith et al.*, 2008] and station precipitation

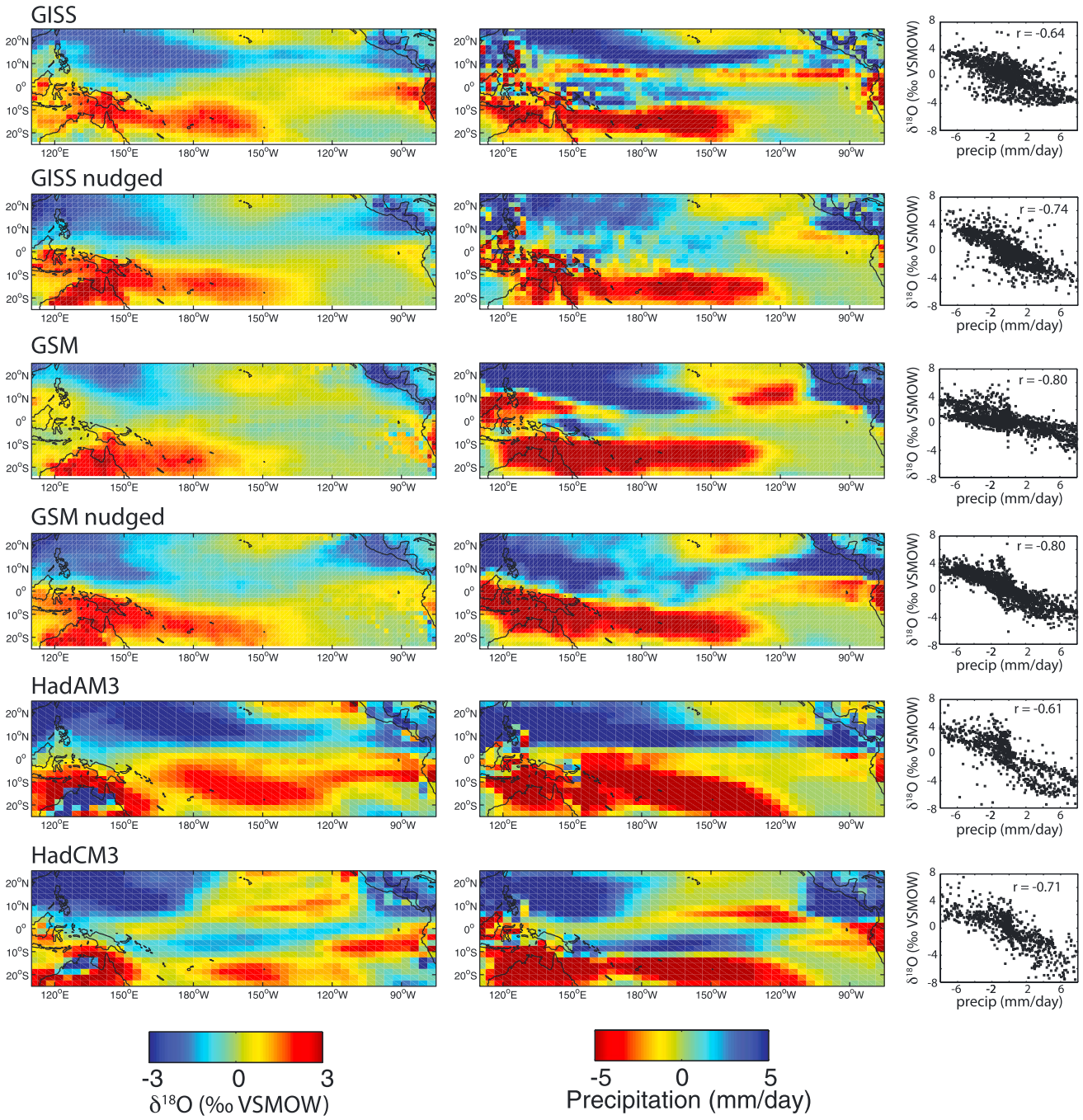

Figure 4. (continued)

observations to create the scatter plots in the right column of Figures 5 and 6.

[20] The El Niño precipitation pattern of wetter conditions over NIÑO3.4 and drier conditions over the Indo-Pacific Warm Pool is present in all simulations. El Niño precipitation and $\delta^{18}O_p$ anomalies are more muted in the GISS nudged and HadCM3 simulations. In the other simulations, El Niño precipitation anomalies are generally too large, and there is a stronger north-south contrast in wet and dry anomalies in the simulations that is not as strongly manifested in observed El Niño anomalies. The magnitude of El Niño drought in the western tropical Pacific also varies strongly from model to model. El Niño patterns of $\delta^{18}O_p$ variability are harder to evaluate against existing $\delta^{18}O_p$ observations, as there are no long time series of $\delta^{18}O_p$ in the region of the strongest isotopic response to ENSO-related SST changes. The available, long (>60 month) time series of $\delta^{18}O_p$ from the tropical Pacific reveal relatively low interannual variability associated with temperature anomalies in NIÑO3.4. However, this may reflect the paucity of the data, as there are only 22 stations with long $\delta^{18}O_p$ time series in or near the tropical Pacific, and none are located in the regions with the strongest simulated El Niño anomalies (Table 2). Clearly more long time series from ENSO-sensitive regions are required to evaluate interannual $\delta^{18}O_p$ variability.

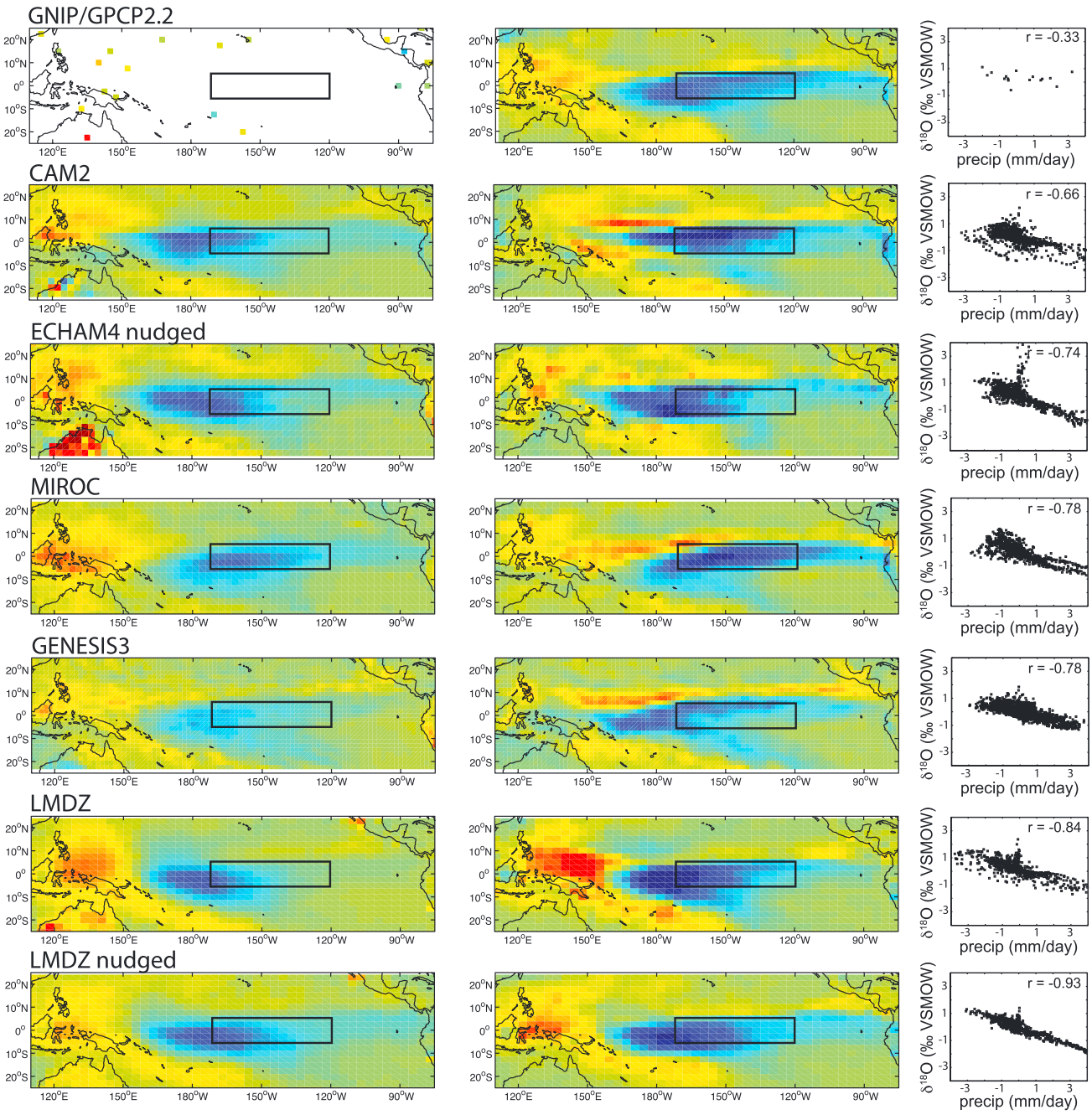

Figure 5. Composite $\delta^{18}O_p$ (left column) and precipitation values (right column) for averaged El Niño months minus the long term average from existing observations and model simulations. Box indicates NIÑO3.4 region. Scatterplots of gridded El Niño $\delta^{18}O_p$ and precipitation anomalies are shown in right column, along with linear correlation coefficients. For scatterplot of observations, we only assess low elevation, near-ocean stations.

[21] In the simulations, El Niño events are characterized by lower $\delta^{18}O_p$ values in a region centered on the equator between 160°E and 150°W. Although the location of the largest negative $\delta^{18}O_p$ anomalies varies by ~10–20° longitudinally, it is generally found at the western end of the NIÑO3.4 region, or west of NIÑO3.4, in 9 of the 12 simulations. This location is displaced to the west of the maximum precipitation anomaly, reflecting systematic changes in the water vapor as it is transported westward by the mean trade winds. This model result is also reflected in contemporary satellite observations [*Noone*, 2012], and underscores the need for models to simulate both precipitation and large-scale atmospheric transport correctly. $\delta^{18}O_p$ values are also higher over the SPCZ and West Pacific warm pool region in 10 of 12 model simulations. In the eastern tropical Pacific, the NIÑO3.4 $\delta^{18}O_p$ signature is weak, except in GSM and HadCM3, which have higher $\delta^{18}O_p$ values, and HadAM3, which has lower $\delta^{18}O_p$ values in this region. Thus, the

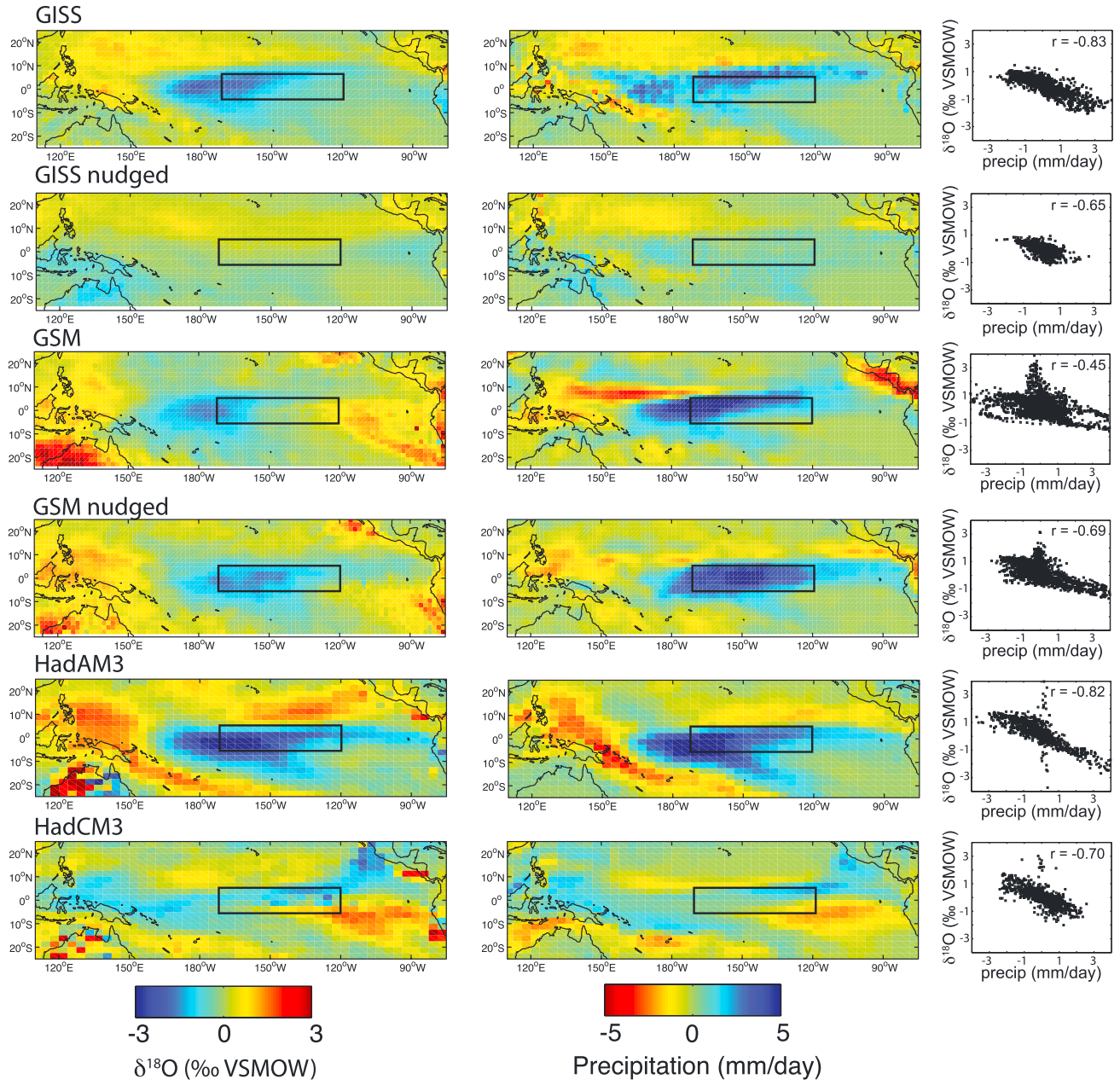

Figure 5. (continued)

strongest isotopic signal related to ENSO (as defined by NIÑO3.4) is found just west of the central equatorial Pacific, displaced westward from peak precipitation anomalies.

[22] This displacement of $\delta^{18}O_p$ anomalies from precipitation anomalies also occurs in the east, where positive precipitation anomalies extend east of negative $\delta^{18}O_p$ anomalies. *Tindall et al.* [2009] ascribed this isotope-precipitation mismatch to relatively smaller increases in precipitation in the drier eastern Pacific during El Niño events (relative to the wetter NIÑO3.4 region). By transforming precipitation anomalies into percentage departures from the mean, *Tindall et al.* [2009] found a much stronger spatial relationship between $\delta^{18}O_p$ and precipitation in the eastern tropical Pacific. We find some of the simulations show similar changes in El Niño precipitation magnitude east of NIÑO3.4 as within NIÑO3.4, indicating that factors other than precipitation amount may be influencing the $\delta^{18}O_p$ values of precipitation in the central and eastern equatorial Pacific on interannual time scales, such as the balance between precipitation and evaporation [*Lee et al.*, 2007] or changes in moisture source regions [*Cole et al.*, 1999]. In fact, GSM and HadCM3 produce positive $\delta^{18}O_p$ anomalies in the eastern tropical Pacific during El Niño events. Although HadCM3 also produces a dry anomaly in this region, GSM has no large decrease in eastern tropical Pacific precipitation that coincides with higher $\delta^{18}O_p$ values during El Niño events.

[23] La Niña precipitation anomalies are similar to observations across the simulations, except in GISS nudged, which has low interannual variability, and HadCM3, which has a stronger meridional pattern of wet and dry anomalies. The isotopic signature associated with ENSO is asymmetric, in that

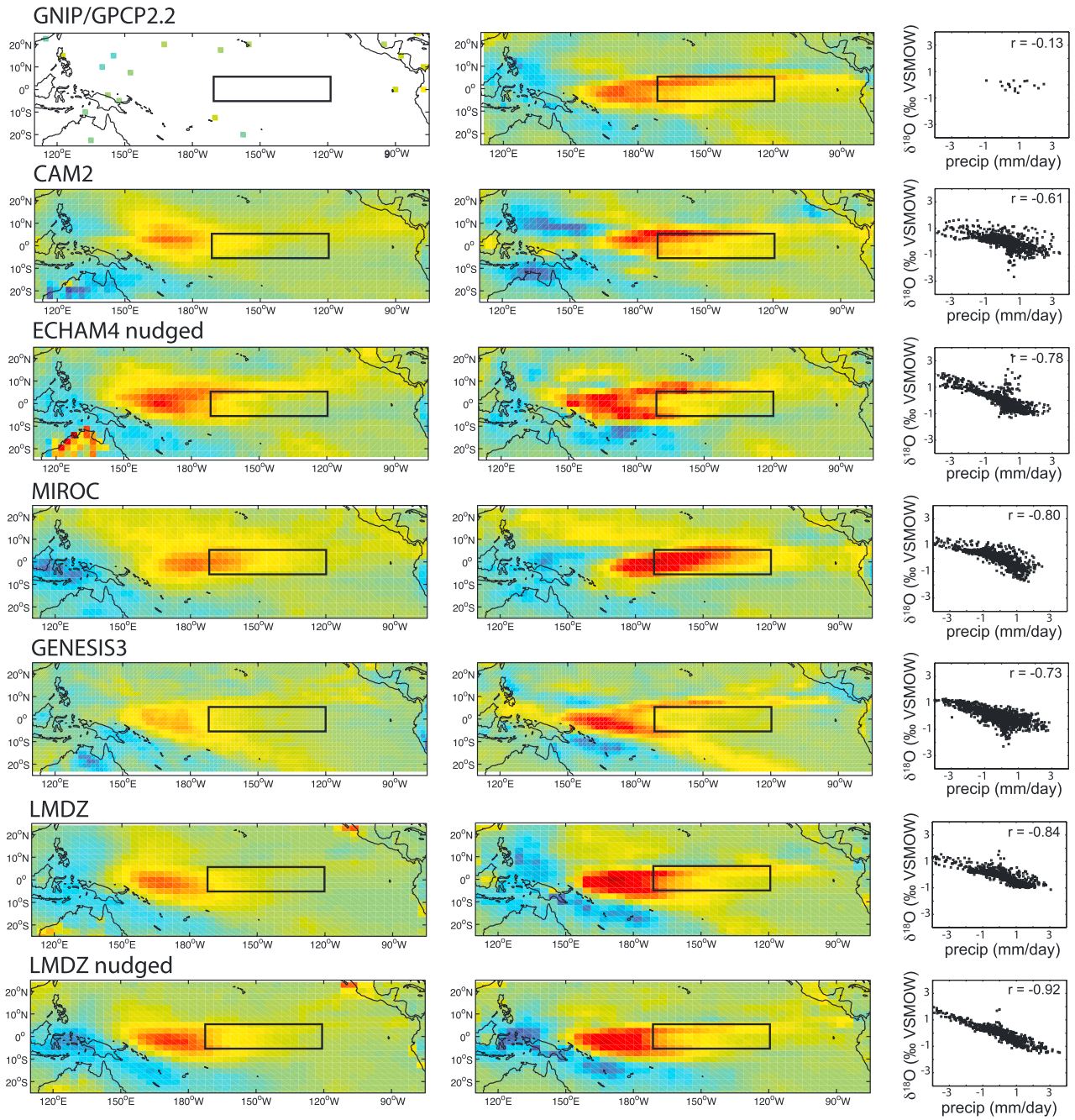

Figure 6. Composite $\delta^{18}O_p$ (left column) and precipitation values (right column) for averaged La Niña months minus the long term average from existing observations and model simulations. Box indicates NIÑO3.4 region. Scatterplots of gridded La Niña $\delta^{18}O_p$ and precipitation anomalies are shown in right column, along with linear correlation coefficients. For scatterplot of observations, we only assess low elevation, near-ocean stations.

during La Niña events, the largest central equatorial Pacific $\delta^{18}O_p$ anomaly is west of the peak El Niño $\delta^{18}O_p$ anomaly in every model except GSM (Figure 6). The magnitude of the La Niña $\delta^{18}O_p$ anomaly in the western Pacific varies from model to model and is largest in MIROC, LMDZ nudged, and GISS. In the far eastern equatorial Pacific, the $\delta^{18}O_p$ response to La Niña is strongest in GSM, GSM nudged, and HadCM3. In the simulations, region-wide La Niña precipitation anomalies are negatively correlated with $\delta^{18}O_p$ anomalies ($r = -0.61$ to -0.92). However, in the observations, the near-ocean La Niña $\delta^{18}O_p$ and precipitation anomalies are not significantly correlated ($r = -0.13$, $N = 17$). Similarly, the correlation coefficients representing the spatial amount effect during El Niño periods ranges from –0.45 to –0.93 in the model simulations, but near ocean observations have a $\delta^{18}O_p$-precipitation correlation coefficient of –0.33 ($N = 17$), also falling outside of the model distribution. This may suggest a limitation in all models with regard to the simulation

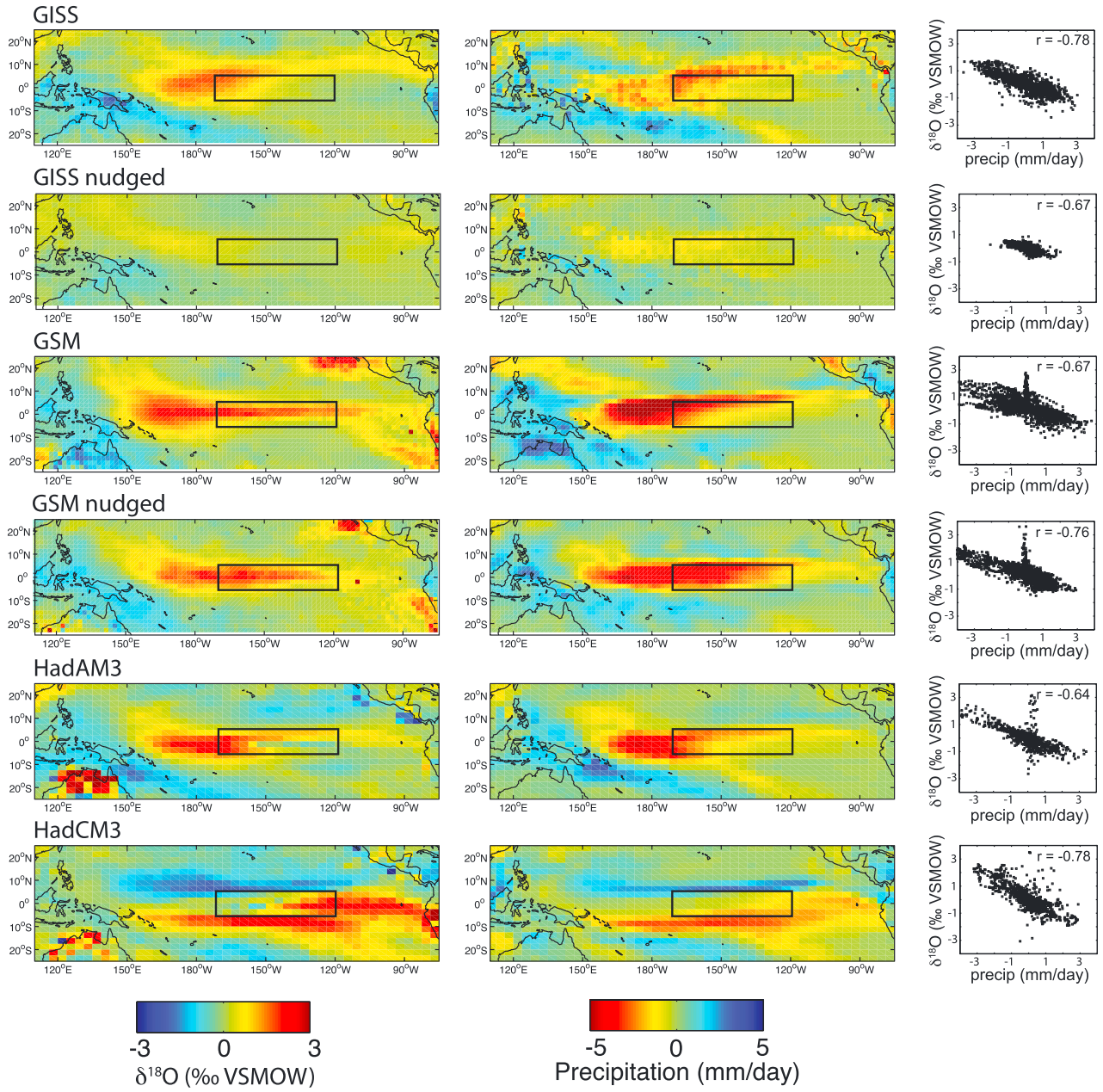

Figure 6. (continued)

of moisture convergence versus convection. However, the lower correlation coefficients in observations may be because of data scarcity, or because the stations are not optimally situated to capture ENSO variability.

3.4. Impact of Nudging on Isotopic Variability

[24] Spectral nudging with reanalysis winds can improve $\delta^{18}O_p$ simulations in some parts of the world, particularly the midlatitudes [*Yoshimura et al.*, 2008; *Risi et al.*, 2010]. However, in the tropics, where sea surface temperatures and cloud processes (the latter being poorly simulated by climate models) are the predominant influence on atmospheric dynamics and precipitation, improving the simulation of large-scale atmospheric circulation is hypothesized to have a limited effect on modeled $\delta^{18}O_p$ [*Yoshimura et al.*, 2008; *Risi et al.*, 2010]. We find that the spatial standard deviations of nudged tropical Pacific precipitation fields are lower (Figure 3a, arrows). Nudged simulations also have reduced precipitation magnitude in the ITCZ and SPCZ (Figure 1). Changes in correlation coefficients and RMSDs of precipitation are distinct to each nudged model, and are not always improved with nudging.

[25] Turning to $\delta^{18}O_p$ values, we find that nudged model simulations of $\delta^{18}O_p$ do diverge from "free" simulations, but are not necessarily improved. Correlation coefficients and RMSDs between mean annual simulated $\delta^{18}O_p$ and observed $\delta^{18}O_p$ are improved in the LMDZ and GISS nudged simulations, but not in the nudged simulation of GSM (Figure 3b). Mean annual standard deviations of $\delta^{18}O_p$ are reduced in GISS and GSM to values lower than observed, but not in LMDZ. Nudged simulations also do not consistently change the strength of $\delta^{18}O_p$-precipitation correlations on seasonal or interannual time scales

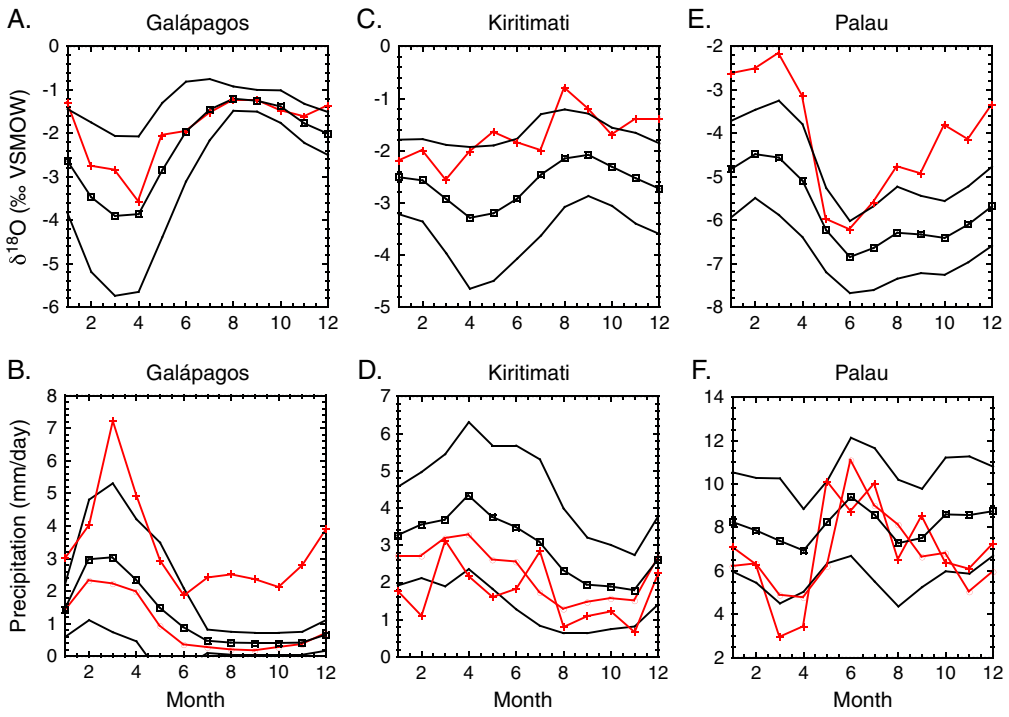

Figure 7. Monthly climatology of precipitation and $\delta^{18}O_p$ values for grids representing sites in the (A–B) eastern (Galápagos), (C–D) the central (Kiritimati), and (E–F) the western (Palau) tropical Pacific Ocean. Red crosses indicate GNIP observational $\delta^{18}O_p$ and precipitation data, red circles indicate GPCP2.2 observations, black markers indicate mean model simulations. Black lines represent one standard deviation of model simulations.

(Figures 4–6), although the magnitude of precipitation and $\delta^{18}O_p$ response to ENSO is reduced in the nudged model simulations compared to free simulations of the same model (Figures 4 and 5). The nudged model simulations do not have drastically different temporal correlation coefficients between monthly $\delta^{18}O_p$ and precipitation (Figure 2), but the nudged simulations tend to have larger areas with more negative correlation coefficients compared to free simulations. The nudging approach introduces an artificial forcing tendency to the wind and temperature fields in the model. Because the tropical precipitation of the nudged simulations is not clearly superior to that of the free simulations, this higher amount effect may simply reflect changes in the behavior of parameterized convection that are acting to return the model state back to a balanced state in a manner akin to geostrophic adjustment. Therefore, it is unclear if a stronger amount effect

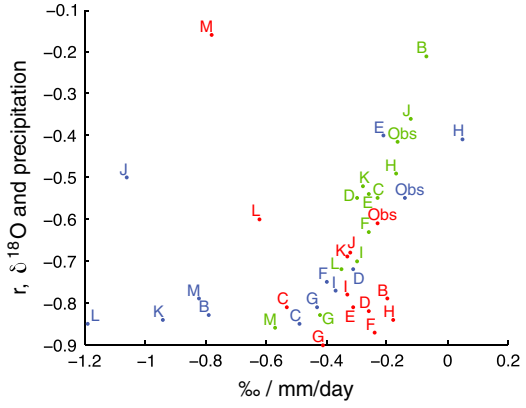

Figure 8. Scatterplot of correlation coefficients between $\delta^{18}O_p$ and precipitation values and regression coefficient for $\delta^{18}O_p$ and precipitation (magnitude of amount effect). Simulations: B: CAM2 C: ECHAM4 nudged D: MIROC E: GENESIS3 F: LMDZ G: LMDZ nudged H: GSM I: GSM nudged J: GISS K: GISS nudged L: HadAM3 M: HadCM3. Blue symbols: Galápagos. Red symbols: Kiritimati. Green symbols: Palau.

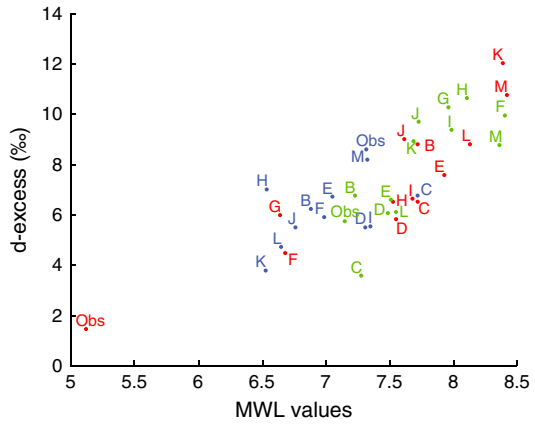

Figure 9. Scatterplot of MWL and d-excess values. Simulations: B: CAM2 C: ECHAM4 nudged D: MIROC E: GENESIS3 F: LMDZ G: LMDZ nudged H: GSM I: GSM nudged J: GISS K: GISS nudged L: HadAM3 M: HadCM3. Blue symbols: Galápagos. Red symbols: Kiritimati. Green symbols: Palau.

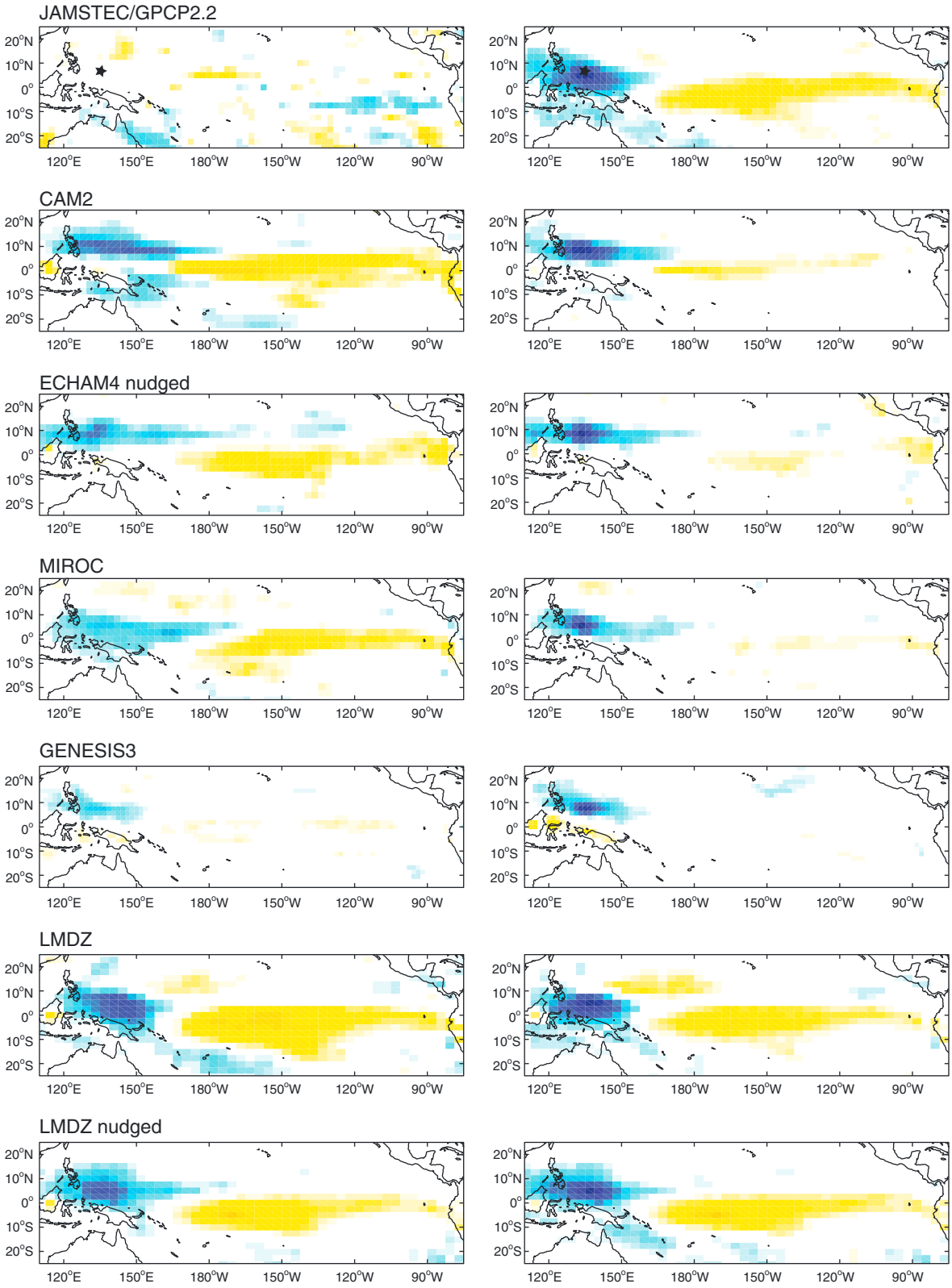

Figure 10. Map of correlation coefficients between monthly anomalies of precipitation and monthly anomalies of $\delta^{18}O_p$ values at the grid cell representing Palau (black star) and monthly anomalies of precipitation across the tropical Pacific. (left) Palau $\delta^{18}O_p$ and gridded precipitation. (right) Palau precipitation and gridded precipitation. Only values that are significant at the two-tailed 95% confidence interval are plotted.

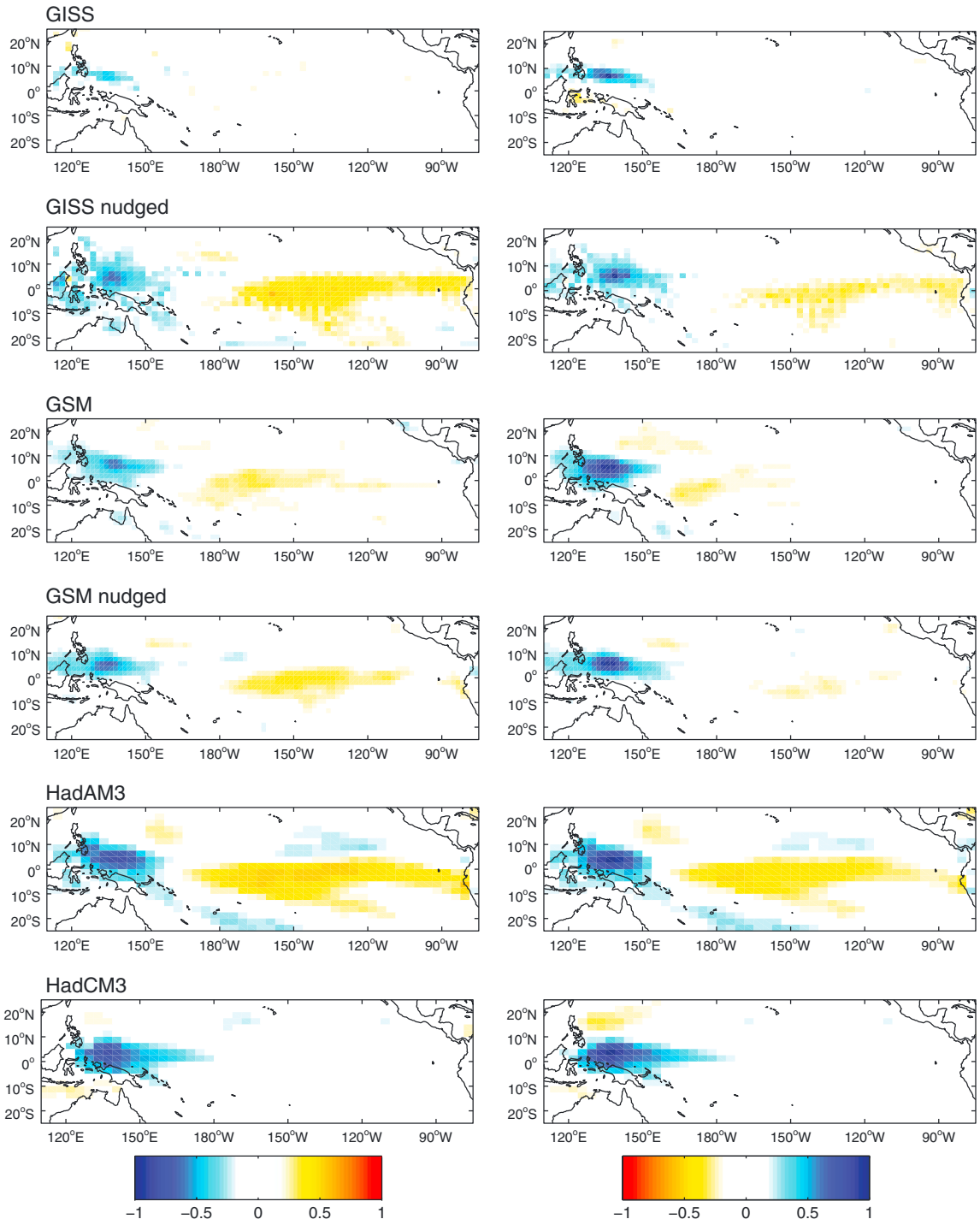

Figure 10. (continued)

in nudged simulations is a model artifact associated with the nudging approach, or if the nudged simulations indicate more profound problems in the treatment of clouds once the wind fields are better constrained.

4. Isotopic Variability in the Eastern, Central, and Western Equatorial Pacific

[26] There is considerable zonal variability in tropical Pacific climate on mean annual, seasonal, and interannual time scales. To investigate how these zonal climate differences translate into stable isotope space, the stable water isotope and precipitation variability at three grid cells across the tropical Pacific that correspond to the Galápagos archipelago, the island of Kiritimati, and Palau are examined. These locations represent the zonal differences in eastern, central, and western equatorial Pacific climate, respectively, and contain well-known proxy isotope records [*Dunbar et al.*, 1994; *Evans et al.*, 1998; *Morimoto et al.*, 2002; *Nurhati et al.*, 2009; *Sachs et al.*, 2009; *Wu and Grottoli*,

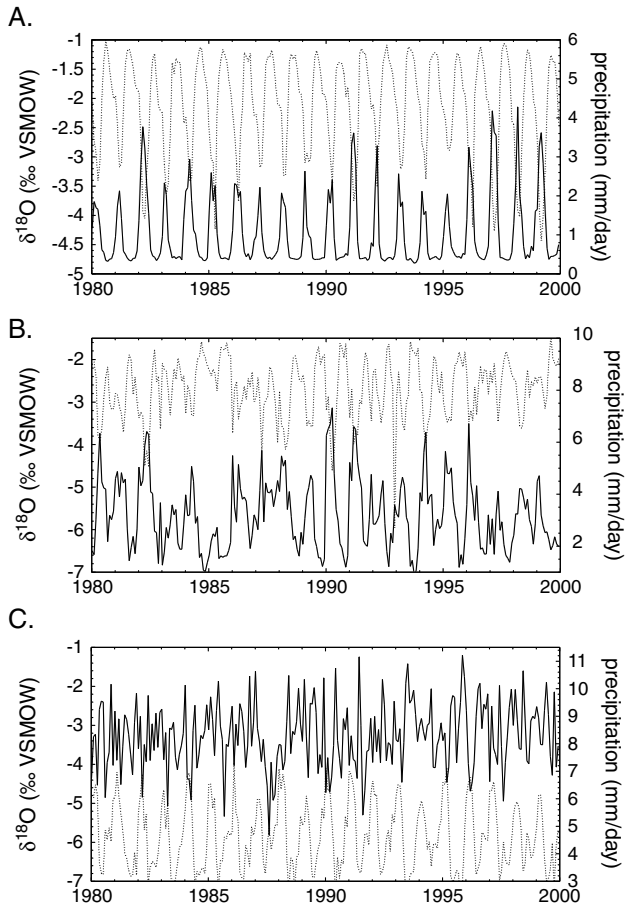

Figure 11. Time series of average model simulations of simulated model $\delta^{18}O_p$ (dotted line) and precipitation (solid line) for (A) Galápagos (B) Kiritimati, and (C) Palau.

2010]. Figure 7 shows the mean climatology of precipitation and $\delta^{18}O_p$ for each site. In both the average model climatology and observations, the Galápagos are driest of the three sites, with a wet season that peaks in February-April and little rain during the rest of the year. The simulations overestimate Galápagos precipitation, particularly the amplitude of the wet season. GNIP station precipitation is much higher than GPCP precipitation for the Galápagos, partly because the GNIP station is located at a higher, relatively moister elevation (194 m); the highlands of the Galápagos receive more precipitation due to orographic penetration of the stable inversion layer and associated stratocumulus cloud deck [*Colinvaux*, 1984]. Along with overestimating wet season precipitation, on average, models simulate $\delta^{18}O_p$ values that are also too negative in the wet season. Generally, Galápagos $\delta^{18}O_p$ values are lowest in observations and simulations from February to April, indicating a climatological amount effect. February and March are the wettest months in the averaged model simulation and in observations, but April has the lowest $\delta^{18}O_p$ values in observations, and the models simulate the lowest $\delta^{18}O_p$ values in March and April.

[27] Like the Galápagos, Kiritimati is also a relatively dry site, but precipitation is higher in the dry period from June to December, reducing the amplitude of the seasonal cycle of precipitation compared to the Galápagos. The climatology of GNIP $\delta^{18}O_p$ from Kiritimati also shows a smaller amplitude seasonal cycle compared to the Galápagos, with the lowest values in January-April, when precipitation peaks, again indicating a climatological amount effect. On average the simulations overestimate precipitation for Kiritimati throughout the year. Along with simulating too much precipitation, the models simulate $\delta^{18}O_p$ values that are too negative. The models also produce a $\delta^{18}O_p$ climatology with a more pronounced seasonal cycle than the limited GNIP data for the site.

[28] Palau, the westernmost and wettest of the three sites, has a wet season coinciding with early boreal summer, from May to July, as it is located at 6°N, the northernmost of the three sites. The model average underestimates the amplitude of the seasonal cycle of precipitation at Palau, and shows the driest months occurring in April and August, while observations show the driest months are March-April and November-December. Like precipitation, average model $\delta^{18}O_p$ values also have a lower amplitude seasonal cycle compared to observed $\delta^{18}O_p$ values. Modeled $\delta^{18}O_p$ values are lowest from June to December, despite the May-July peak in precipitation, highlighting the reduced importance of local precipitation amount on $\delta^{18}O_p$ values at this site.

[29] The strength of the amount effect varies across model simulations at the three tropical Pacific sites considered here, and is generally overestimated by all simulations. Figure 8 shows the correlation coefficient between monthly $\delta^{18}O_p$ and precipitation values and the linear regression coefficient between monthly $\delta^{18}O_p$ and precipitation values (in ‰/mm/d), at Galápagos, Kiritimati and Palau for each model simulation and observations. Correlation and regression coefficients from station observations are similar for the three sites, with regression coefficients of ~ –0.2‰ /mm/d, and correlation coefficients that range between –0.4 and –0.6. However, the correlation and regression coefficients vary widely from simulation to simulation, and are too strong overall, as apparent in Figures 1 and 2. Many models simulate the strongest amount effect magnitude for the Galápagos, whereas the weakest modeled amount effect is at Palau.

[30] The relationships between δD_p and $\delta^{18}O_p$ at each site can provide additional information on the relationship between water isotopes and climate, particularly the impact of kinetic effects related to evaporation [*Gat*, 1996]. Figure 9 shows the meteoric water lines and deuterium excess values derived from the linear regression lines of both simulated and observed monthly $\delta^{18}O_p$ and δD_p values. Simulated meteoric water lines (MWLs) and d-excess values for Palau, Kiritimati, and Galápagos overlap one another and cluster around the global average values of 8 and 10 for the MWL and deuterium excess (d-excess), respectively. Simulated MWL slopes and d-excess values for the Galápagos are lower compared to values for Palau and Kiritimati. Compared to observations, the simulations underestimate MWL and d-excess values in the Galápagos. At Palau, simulated MWL and d-excess values also diverge from observations, with the simulations overestimating MWL and d-excess values. Simulated MWL and d-excess values for Kiritimati diverge most strongly from observations, and are much higher than observed values.

[31] Lower local MWL and d-excess values, such as those at Kiritimati, may indicate a stronger evaporative influence on falling rain [*Jouzel*, 1986; *Gat*, 1996]. The simulations of higher MWL and d-excess values, compared to the observed values at Kiritimati, suggests the models do not produce

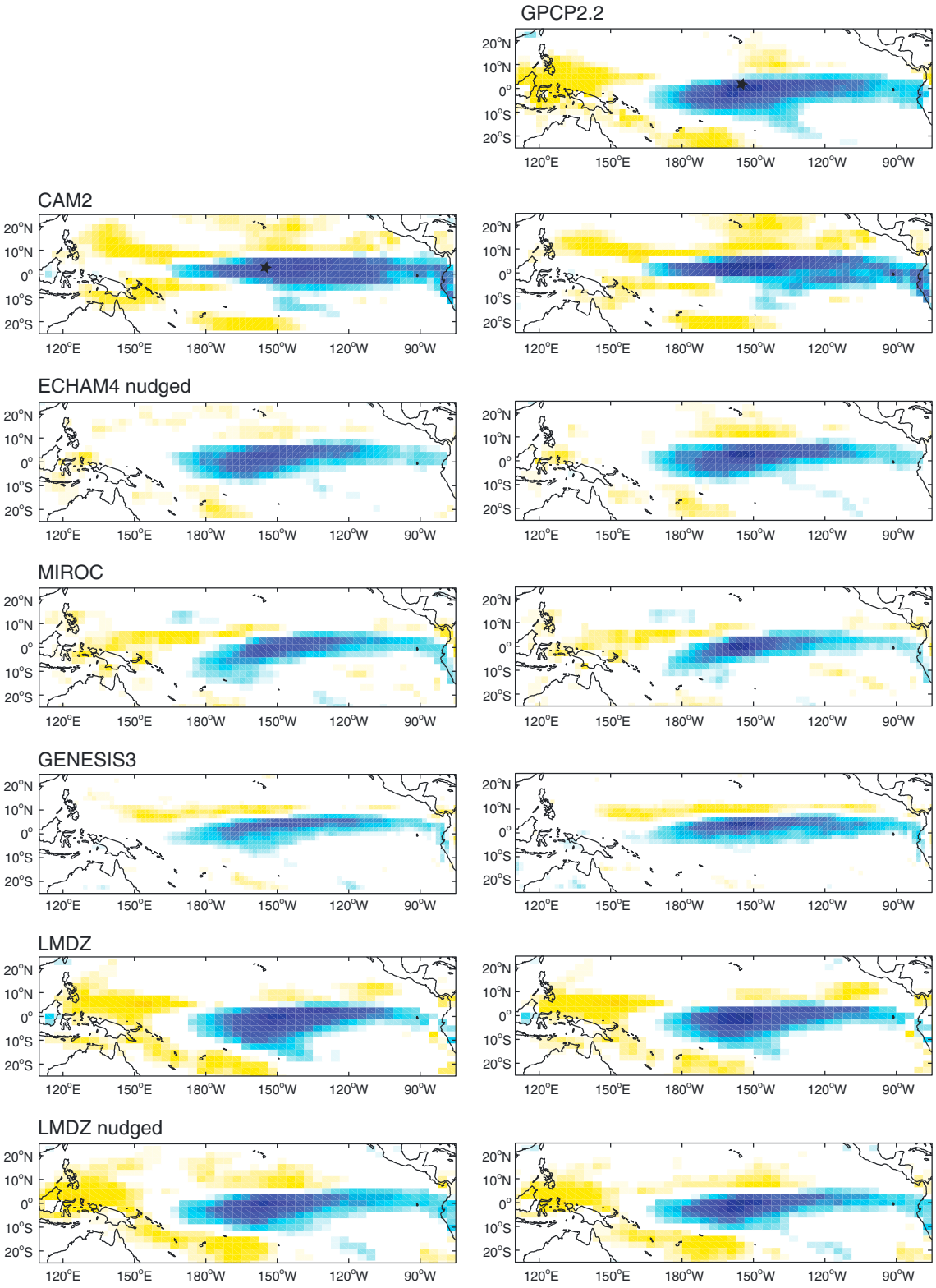

Figure 12. Map of correlation coefficients between monthly anomalies of precipitation and monthly anomalies of $\delta^{18}O_p$ values at the grid cell representing Kiritimati (black star) and monthly anomalies of precipitation across the tropical Pacific. (left) Kiritimati $\delta^{18}O_p$ and gridded precipitation. (right) Kiritimati precipitation and gridded precipitation. Only values that are significant at the two-tailed 95% confidence interval are plotted.

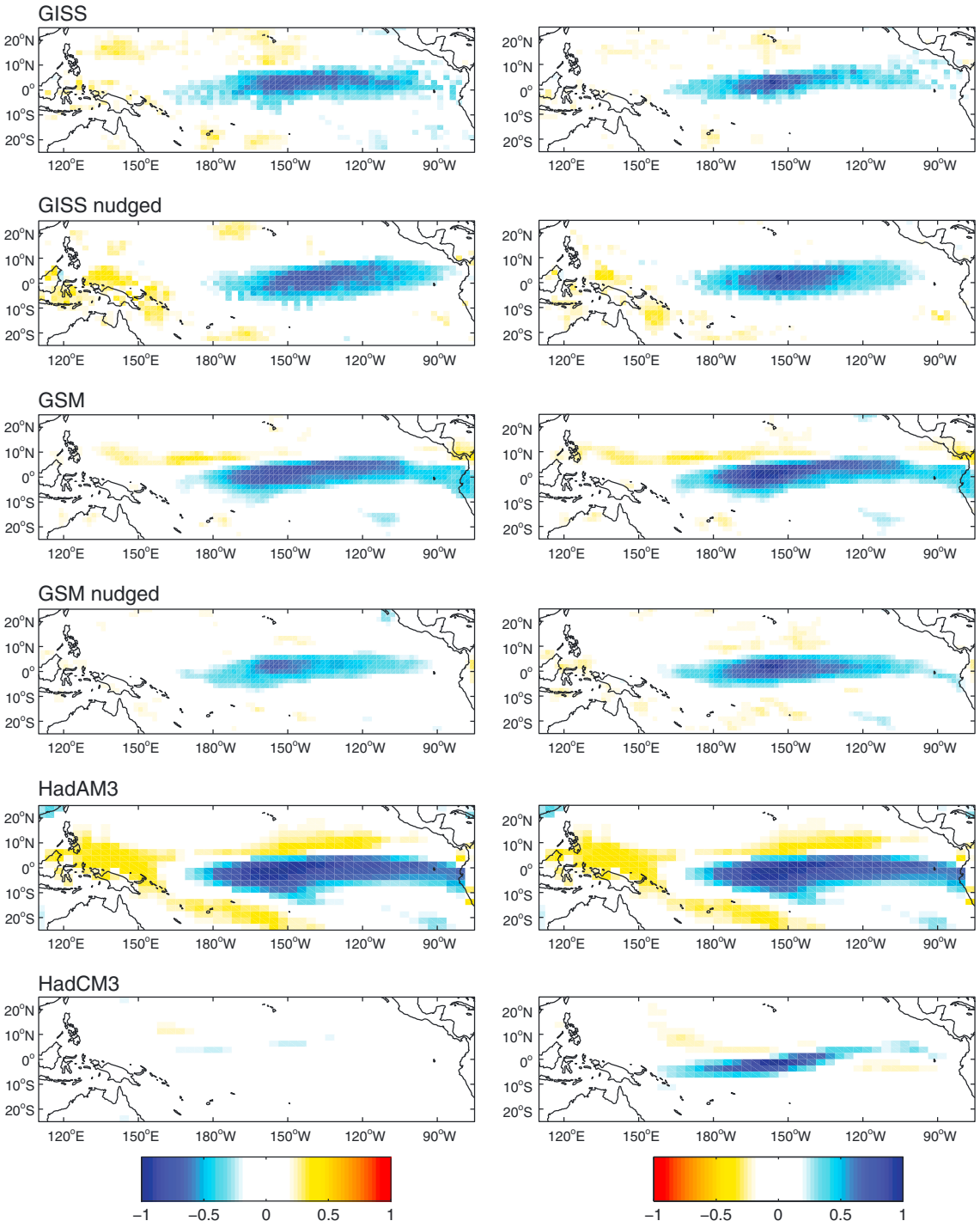

Figure 12. (continued)

enough rain evaporation in the central tropical Pacific. The same model deficiency occurs in Palau, where simulated local MWL and d-excess values are higher than those observed. In the Galápagos, simulated local MWL and d-excess values are lower than observed values, suggesting the models may produce too much evaporation in this region. However, the Galápagos GNIP station is located in a higher-elevation, more humid site that may have reduced evaporation compared to sea level. An additional time series of precipitation isotopes from near sea level in the Galápagos would be useful to explore altitude-induced evaporative effects in the islands.

4.1. Local δ^{18}Op Variability: Local or Regional Hydroclimate Proxy?

[32] Recent analyses of precipitation and $\delta^{18}O_p$ values in the western tropical Pacific and parts of monsoon Asia have demonstrated that local $\delta^{18}O_p$ and local precipitation amount often do not share a strong relationship [*Cobb et al.*, 2007;

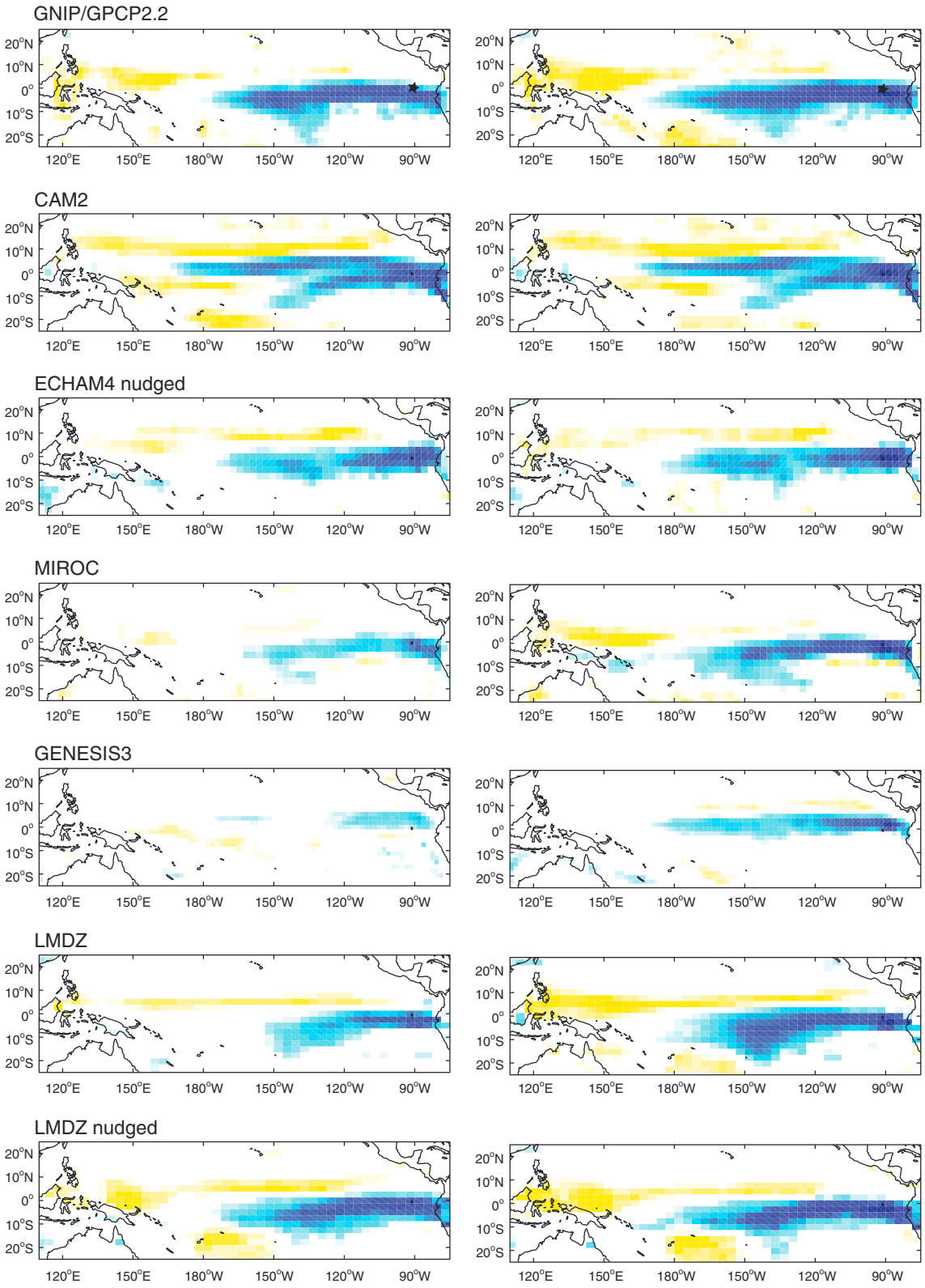

Figure 13. Map of correlation coefficients between monthly anomalies of precipitation and monthly anomalies of $\delta^{18}O_p$ values at the grid cell representing Galápagos (black star) and monthly anomalies of precipitation across the tropical Pacific. (left) Galápagos $\delta^{18}O_p$ and gridded precipitation. (right) Galápagos precipitation and gridded precipitation. Only values that are significant at the two-tailed 95% confidence interval are plotted.

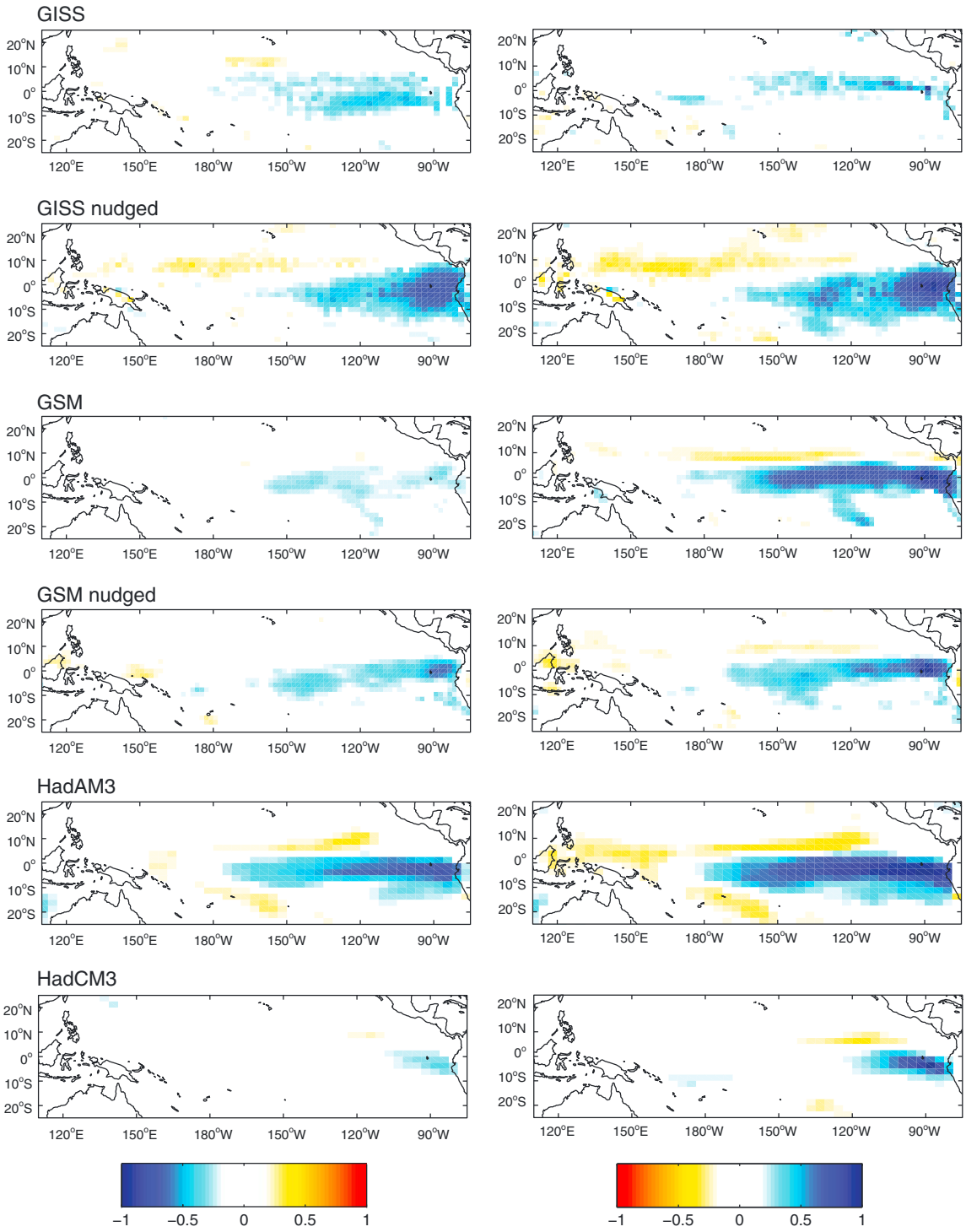

Figure 13. (continued)

Kurita et al., 2009; *LeGrande and Schmidt*, 2009; *Dayem et al.*, 2010; *Moerman et al.*, 2013]. Rather, vapor transport history and the degree of vapor parcel distillation are implicated as the main controls on $\delta^{18}O_p$ variability, such that western tropical Pacific and east Asian $\delta^{18}O_p$ are variables that reflects aspects of regional-scale atmospheric circulation, rather than just local rainfall amount [*Cobb et al.*, 2007; *Kurita et al.*, 2009; *LeGrande and Schmidt*, 2009; *Dayem et al.*, 2010; *Moerman et al.*, 2013]. In this section, we investigate monthly anomalies of $\delta^{18}O_p$ and precipitation variability at each site to assess how local $\delta^{18}O_p$ and precipitation values relate to precipitation variability across the entire tropical Pacific basin.

[33] Given recent observations and modeling results for other parts of the western tropical Pacific, we hypothesize that simulated $\delta^{18}O_p$ at Palau will be better correlated to

regional, rather than local precipitation [*Kurita et al*., 2009]. Palau precipitation, on the other hand, will likely only correlate with local precipitation, rather than basin-wide precipitation anomalies. We find that the relationship between Palau $\delta^{18}O_p$, Palau precipitation, and tropical Pacific precipitation is not consistent among model simulations (Figure 10). In the 7 of out the 12 simulations and 3 out of the 4 nudged simulations—CAM2, ECHAM4, MIROC, GISS nudged, GSM, GSM nudged, and HadAM3—the relationship between Palau $\delta^{18}O_p$ and basin-wide precipitation is stronger than the relationship between Palau precipitation and basin-wide precipitation, especially in the central and eastern tropical Pacific. In GENESIS, GISS, and HadCM3, both Palau $\delta^{18}O_p$ and precipitation are only correlated with local precipitation. In LMDZ and LMDZ nudged, both $\delta^{18}O_p$ and precipitation at Palau have strong relationships with precipitation across the tropical Pacific. None of the simulations accurately reproduce the observed lack of relationship between Palau $\delta^{18}O_p$ anomalies and local, as well as large-scale, precipitation anomalies. Palau is located near the eastern edge of the warm pool and provides a particular challenge for models to capture precipitation and transport processes near steep gradients in SST. Indeed, the lack of a relationship between large-scale tropical Pacific precipitation and Palau $\delta^{18}O_p$ in the observational data suggests the model simulations broadly fail to capture the hydrology of the region.

[34] Recent analysis of a 4 year data set of monthly $\delta^{18}O_p$ from Palau demonstrates that local $\delta^{18}O_p$ is correlated with regional (rather than local) precipitation and large-scale convergence and divergence associated with the seasonal march of the ITCZ [*Kurita et al*. 2009]. However, as seen in Figure 10, observed monthly anomalies of $\delta^{18}O_p$ at Palau are also not correlated with regional precipitation anomalies; overall correlations are generally weak across the western Pacific. Strong correlations are observed when we include the seasonal cycle in the $\delta^{18}O_p$ data, correlating monthly $\delta^{18}O_p$ and monthly tropical Pacific precipitation, rather than the monthly anomalies (see Figure S1 in the supporting information). In this case, we find that Palau $\delta^{18}O_p$ is negatively correlated with precipitation north of the equator across the tropical Pacific, and positively correlated with precipitation south of the equator across the tropical Pacific. All model simulations also capture this north-south pattern of correlations when the seasonal cycle is included in the precipitation and $\delta^{18}O_p$ time series, with the exception of the "free" simulations of GISS and GSM.

[35] The reason for the stronger relationship between monthly Palau $\delta^{18}O_p$ and regional, rather than local, precipitation is thought to relate to changes in large-scale convergence and divergence [*Kurita et al*. 2009]. These atmospheric variables share a relationship with $\delta^{18}O_p$ as they can influence water vapor isotope values through changes in the degree of vapor parcel distillation, and upwind rain evaporation [*Lawrence et al*., 2004; *Risi et al*., 2010]. As divergence and convergence are highly seasonal in this region, they likely impart a stronger seasonal cycle to Palau $\delta^{18}O_p$ values, whereas precipitation lacks strong seasonality and is defined by interannual variability (Figure 11).

[36] Both $\delta^{18}O_p$ and precipitation anomalies at Kiritimati are strongly correlated with precipitation across the central and eastern equatorial Pacific in every model simulation except HadCM3, in which case only local precipitation, not $\delta^{18}O_p$, is correlated with central equatorial Pacific rainfall (Figure 12). Although both $\delta^{18}O_p$ and precipitation at Kiritimati are highly correlated with precipitation across a broad swath of the central and eastern equatorial Pacific, the relationship between $\delta^{18}O_p$ and precipitation at Kiritimati and western tropical Pacific precipitation varies more from model to model. There is a strong relationship, with increased precipitation and lower $\delta^{18}O_p$ values at Kiritimati coinciding with decreased precipitation and higher $\delta^{18}O_p$ values in the western tropical Pacific, in CAM2, MIROC, LMDZ, LMDZ nudged, and HadAM3. In ECHAM4 nudged, GENESIS, GISS, GISS nudged, GSM, GSM nudged, and HadCM3 there is no relationship between either Kiritimati $\delta^{18}O_p$ or Kiritimati precipitation and western tropical Pacific precipitation, suggesting controls on $\delta^{18}O_p$ are related more to precipitation than atmospheric circulation.

[37] The observed spatial relationship between Kiritimati precipitation anomalies and monthly precipitation anomalies across the tropical Pacific includes positive correlation coefficients across the central and eastern tropical Pacific and negative correlations in the western equatorial Pacific. As the Kiritimati GNIP $\delta^{18}O_p$ time series is from the early 1960s, prior to the period of satellite observations, we are unable to compare observed $\delta^{18}O_p$ values with GPCP2.2 data. However, based on our comparison to observed precipitation, CAM2, MIROC, LMDZ, LMDZ nudged, and HadAM3 seem to best simulate the relationship between local Kiritimati precipitation variability and precipitation across the tropical Pacific. These simulations all have a negative correlation between Kiritmati precipitation anomalies and western equatorial Pacific precipitation anomalies. Given the strong coherence between modeled precipitation and $\delta^{18}O_p$ in Kiritimati, we conclude $\delta^{18}O_p$ in the central equatorial Pacific is a proxy for local rainfall amount. Yet, as observed by the strong correlation coefficients between both $\delta^{18}O_p$ and precipitation at Kiritimati with basin-scale precipitation in the simulations, both $\delta^{18}O_p$ and precipitation may be considered proxies for large-scale atmospheric variability as well. This is because interannual variability in local precipitation amount at Kiritimati is driven by changes to horizontal convergence associated with large-scale Walker Circulation, which also modulates hydroclimate across much of the tropical Pacific.

[38] Galápagos precipitation and $\delta^{18}O_p$ values are correlated with precipitation in the eastern equatorial Pacific in all model simulations. However, the relationship between both Galápagos precipitation and $\delta^{18}O_p$ and west-central to western tropical Pacific precipitation is generally weak, and completely absent in GENESIS3, GISS, GSM, GSM nudged, and HadCM3. In MIROC, LMDZ, LMDZ nudged, GISS nudged, and HadAM3, Galápagos precipitation has a stronger relationship with western Pacific precipitation compared to Galápagos $\delta^{18}O_p$. Furthermore, in GENESIS3, GSM, and GSM nudged, there are stronger correlation coefficients between Galápagos precipitation and precipitation further west relative to the correlation coefficients between Galápagos $\delta^{18}O_p$ and gridded precipitation. That is, the relationship between Galápagos $\delta^{18}O_p$ and large-scale precipitation is more confined to the far eastern equatorial Pacific, compared to the relationship between Galápagos precipitation and basin-wide precipitation. Thus, in the eastern tropical Pacific,

model simulations suggest precipitation, rather than $\delta^{18}O_p$, may be a better indicator of basin-scale hydroclimatic variability, while $\delta^{18}O_p$ reflects regional precipitation.

[39] Galápagos precipitation observations from the GPCP2.2 data set indicate a strong, positive relationship between Galápagos precipitation anomalies and eastern to central equatorial Pacific precipitation anomalies (Figure 13). Galápagos precipitation anomalies also have a significant negative correlation with precipitation in the western-central equatorial Pacific, centered around 150°E. A similar spatial pattern of significant correlation coefficients is also found between monthly anomalies of GNIP Galápagos $\delta^{18}O_p$ data and precipitation. The relationship between Galápagos precipitation and tropical Pacific precipitation is slightly stronger in the western equatorial Pacific and SPCZ compared to the relationship between Galápagos $\delta^{18}O_p$ and precipitation in these regions. Thus, there is a stronger relationship between Galápagos precipitation and remote tropical Pacific precipitation in eight of the twelve model simulations that is also weakly expressed in observations. Thus, in the eastern equatorial Pacific, direct proxies of precipitation amount, rather than proxies for $\delta^{18}O_p$, may serve as more robust indicators of large-scale tropical Pacific precipitation.

5. Conclusions

[40] The distribution of simulated precipitation and $\delta^{18}O_p$ values is useful for assessing the climatic factors that drive $\delta^{18}O_p$ variability in the tropical Pacific, especially as this region lacks long, continuous observations of $\delta^{18}O_p$. An assessment of the 12 model simulations archived in the SWING2 database shows those simulations with the most accurate mean annual precipitation patterns across the tropical Pacific are not the simulations with the best mean annual $\delta^{18}O_p$, patterns, indicating factors beyond precipitation amount wield a large influence on $\delta^{18}O_p$ across this region in model simulations. Simulations nudged with reanalysis winds have improved precipitation magnitude and reduced mean annual standard deviations of precipitation across the tropical Pacific to values closer to observations. However, the impact of nudging on mean annual $\delta^{18}O_p$ is small. There is evidence that overall model simulations may underestimate evaporation of falling rain in the western and central equatorial Pacific, and may produce too much rain evaporation in the eastern equatorial Pacific. Furthermore, a more detailed isotopic parameterization for raindrop equilibration with subcloud vapor may impart a much reduced amount effect, in closer agreement with observations.

[41] The similarity or dissimilarity of precipitation and isotope distributions inform the nature of hydroclimate signal archived in site-specific $\delta^{18}O_p$ records from across the tropical Pacific. Model simulations support the observational conclusion that in the western tropical Pacific, monthly $\delta^{18}O_p$ anomalies are not driven by local precipitation anomalies. Across the simulations, simulated $\delta^{18}O_p$ in Palau has a strong seasonal cycle, whereas precipitation is dominated by interannual variability, causing a weak local amount effect. In many model simulations, Palau $\delta^{18}O_p$ anomalies are correlated with precipitation throughout the western, central, and eastern equatorial Pacific, whereas Palau precipitation anomalies are not. However, other simulations only show a weak local relationship between Palau $\delta^{18}O_p$ anomalies and precipitation anomalies. Furthermore, a strong relationship between Palau $\delta^{18}O_p$ anomalies and basin-scale precipitation anomalies is not observed in the 4 year data set of monthly $\delta^{18}O_p$ anomalies from Palau. These results highlight the inadequacy of simply attributing $\delta^{18}O_p$ variability in the western equatorial Pacific purely to local or large-scale precipitation variability.

[42] In the central equatorial Pacific, Kiritimati $\delta^{18}O_p$ is strongly correlated with local precipitation amount, both seasonally and interannually. Local precipitation is strongly influenced by interannual changes in the large-scale Walker Circulation, rendering both precipitation and $\delta^{18}O_p$ proxies for precipitation variability across the tropical Pacific. However, across the model simulations, the strongest and most consistent precipitation signal reflected in Kiritimati $\delta^{18}O_p$ is confined to the central and eastern equatorial Pacific. Although model agreement regarding the strong relationship between Kiritimati $\delta^{18}O_p$ and large-scale precipitation variability is promising, we still lack long, continuous $\delta^{18}O_p$ data to adequately validate $\delta^{18}O_p$ simulations.

[43] In the eastern equatorial Pacific, both Galápagos $\delta^{18}O_p$ and precipitation have a strong seasonal cycle and the strongest climatological correlation of the three sites. On interannual time scales, Galápagos precipitation anomalies have a stronger, more spatially extensive relationship with precipitation anomalies in the central and western tropical Pacific compared to Galápagos $\delta^{18}O_p$ anomalies in many simulations and more subtly in observations. Thus, model simulations would suggest that in the Galápagos, direct proxies for precipitation may better reflect large-scale tropical Pacific precipitation patterns, whereas $\delta^{18}O_p$ will more closely reflect regional, eastern equatorial Pacific precipitation variability.

[44] Although model agreement lends insight into the local and regional drivers of $\delta^{18}O_p$ variability in the tropical Pacific, ultimately we require improved observations to test these hypotheses. Unfortunately, the tropical Pacific still lacks the decades-long, continuous time series of $\delta^{18}O_p$ needed to understand the isotopic response to key elements of the climate system, especially ENSO. Furthermore, limited or nonexistent ultra-high-resolution records of daily $\delta^{18}O_p$ and $\delta^{18}O$ vapor values hinders our quantitative understanding of the underlying physics of the amount effect, or the other variables that drive $\delta^{18}O_p$ variability. Future development of such data sets and rigorous hypothesis testing of the conclusions drawn from the model distributions presented here is essential to advance our quantitative understanding of the factors that drive $\delta^{18}O_p$ variability in the tropical Pacific.

[45] Finally, insights into the relationship between climate and $\delta^{18}O_p$ in the tropical Pacific are useful for assessing paleoclimatic proxy potential, but they are not the only factors to consider when interpreting water isotope-based paleoclimate proxies across the tropical Pacific. Most water isotope proxies are influenced not only by the $\delta^{18}O$ value of rainfall, but other important variables, such as residence time and evaporation in the case of lake water, and advection of water masses in the case of coral records. When assessing the hydroclimate proxy potential of water isotope-based paleoclimate records, all these influences must be taken into account, which may serve to enhance or degrade the hydroclimate signal archived in the water isotope proxy. This work only addresses one aspect of the complex history

of water isotope-based proxies, but it is an essential first step toward developing accurate climate-water isotope relationships for the past and the present.

[46] **Acknowledgments.** This work was supported by NSF-AGS-PF 1049664 to JLC, NSF ATM-0645291 to KMC, and NASA awards NNX08AR23G and 07-NEWS07-0020 to DN. We thank E. DiLorenzo for assisting with access to model archives.

References

Adler, R. F., et al. (2003), The version-2 global precipitation climatology project (GPCP) monthly precipitation analysis (1979-present), *J. Hydrometeorol.*, *4*(6), 1147–1167.

Anchukaitis, K. J., M. N. Evans, N. T. Wheelwright, and D. P. Schrag (2008), Stable isotope chronology and climate signal calibration in neotropical montane cloud forest trees, *J. Geophys. Res.*, *113*, G03030, doi:10.1029/2007JG000613.

Araguas-Araguas, L., K. Froehlich, and K. Rozanski (1998), Stable isotope composition of precipitation over southeast Asia, *J. Geophys. Res. Atmos.*, *103*(D22), 28721–28742.

Berkelhammer, M., C. Risi, N. Kurita, and D. Noone (2012), The moisture source sequence of the Madden-Julian Oscillation as derived from satellite retrievals of HDO and H2O, *J. Geophys. Res.*, *117*, D03106, doi:10.1029/2011JD016803.

Brown, J., I. Simmonds, and D. Noone (2006), Modeling $\delta^{18}O$ in tropical precipitation and the surface ocean for present-day climate, *J. Geophys. Res.*, *111*, D05105, doi:10.1029/2004JD005611.

Cobb, K. M., J. F. Adkins, J. W. Partin, and B. Clark (2007), Regional-scale climate influences on temporal variations of rainwater and cave dripwater oxygen isotopes in northern Borneo, *Earth Planet. Sci. Lett.*, *263*(3-4), 207–220.

Cole, J. E., D. Rind, R. S. Webb, J. Jouzel, and R. Healy (1999), Climatic controls on interannual variability of precipitation $\delta^{18}O$: Simulated influence of temperature, precipitation amount, and vapor source region, *J. Geophys. Res.*, *104*(D12), 14223–14235, doi:10.1029/1999JD900182.

Colinvaux, P. A. (1984), The Galapagos climate: Present and past, in *Key Environments: Galapagos*, edited by R. Perry, pp. 55–69, Pergamon Press, Oxford.

Dai, A. (2006), Precipitation characteristics in eighteen coupled climate models, *J. Climate*, *19*(18), 4605–4630.

Dansgaard, W. (1964), Stable isotopes in precipitation, *Tellus*, *16*(4), 436–468.

Dayem, K. E., P. Molnar, D. S. Battisti, and G. H. Roe (2010), Lessons learned from oxygen isotopes in modern precipitation applied to interpretation of speleothem records of paleoclimate from eastern Asia, *Earth Planet. Sci. Lett.*, *295*(1-2), 219–230.

Dunbar, R. B., G. M. Wellington, M. W. Colgan, and P. W. Glynn (1994), Eastern Pacific SST since 1600 AD the $\delta^{18}O$ record of climate variability in Galápagos corals, *Paleoceanogr.*, *9*(2), 291–315.

Evans, M. N., R. G. Fairbanks, and J. L. Rubenstone (1998), A proxy for ENSO teleconnections, *Nature*, *394*, 732–733.

Feng, X. H., A. M. Faiia, and E. S. Posmentier (2009), Seasonality of isotopes in precipitation: A global perspective, *J. Geophys. Res.*, *114*, D08116, doi:10.1029/2008JD011279.

Gat, J. R. (1996), Oxygen and hydrogen isotopes in the hydrologic cycle, *Annu. Rev. Earth Planet. Sci.*, *24*, 225–262.

Hoffmann, G., M. Werner, and M. Heimann (1998), Water isotope module of the ECHAM atmospheric general circulation model: A study on timescales from days to several years, *J. Geophys. Res.*, *103*(D14), 16871–16896, doi:10.1029/98JD00423.

IAEA/WMO (2006), International Atomic Energy Agency/World Meteorological Organization Global Network for Isotopes in Precipitation, The GNIP Database, edited, Accessible at: http://www.iaea.org/water.

Joussaume, S., R. Sadourny, and J. Jouzel (1984), A general circulation model of water isotope cycles in the atmosphere, *Nature*, *311*(5981), 24–29.

Jouzel, J. (1986), Isotopes in cloud physics: Multiphase and multistage condensation processes, in *Handbook of Environmental Isotope Geochemsitry*, edited by P. Fritz, and J. C. Fontes, pp. 61–112, Elsevier, New York.

Jouzel, J., G. Hoffmann, R. D. Koster, and V. Masson (2000), Water isotopes in precipitation: data/model comparison for present-day and past climates, *Quat. Sci. Rev.*, *19*(1-5), 363–379.

Kurita, N., K. Ichiyanagi, J. Matsumoto, M. D. Yamanaka, and T. Ohata (2009), The relationship between the isotopic content of precipitation and the precipitation amount in tropical regions, *J. Geochem. Explor.*, *102*(3), 113–122.

Kurita, N., D. Noone, C. Risi, G. A. Schmidt, H. Yamada, and K. Yoneyama (2011), Intraseasonal isotopic variation associated with the Madden-Julian Oscillation, *J. Geophys. Res.*, *116*, D24101, doi:10.1029/2010JD015209.

Lawrence, J. R., S. D. Gedzelman, D. Dexheimer, H. K. Cho, G. D. Carrie, R. Gasparini, C. R. Anderson, K. P. Bowman, and M. I. Biggerstaff (2004), Stable isotopic composition of water vapor in the tropics, *J. Geophys. Res.*, *109*, D06115, doi:10.1029/2003JD004046.

Lee, J. E., and I. Fung (2007), "Amount effect" of water isotopes and quantitative analysis of post-condensation processes, *Hydrol. Process.*, doi:10.1002/hyp.6637.

Lee, J. E., I. Fung, D. J. DePaolo, and C. C. Henning (2007), Analysis of the global distribution of water isotopes using the NCAR atmospheric general circulation model, *J. Geophys. Res.*, *112*, D16306, doi:10.1029/2006JD007657.

Lee, J. E., R. Pierrehumbert, A. Swann, and B. R. Lintner (2009), Sensitivity of stable water isotopic values to convective parameterization schemes, *Geophys. Res. Lett.*, *36*, L23801, doi:10.1029/2009GL040880.

LeGrande, A. N., and G. A. Schmidt (2009), Sources of Holocene variability of oxygen isotopes in paleoclimate archives, *Clim. Past*, *5*(3), 441–455.

Lin, J. L. (2007), The double-ITCZ problem in IPCC AR4 coupled GCMs: Ocean-atmosphere feedback analysis, *J. Climate*, *20*(18), 4497–4525.

Mathieu, R., D. Pollard, J. E. Cole, J. W. C. White, R. S. Webb, and S. L. Thompson (2002), Simulation of stable water isotope variations by the GENESIS GCM for modern conditions, *J. Geophys. Res.*, *107*(D4), 4037, doi:10.1029/2001JD900255.

Moerman, J., K. M. Cobb, and B. Clark (2013), Climate controls on rainwater oxygen isotopic variability in northern Borneo on sub-seasonal to interannual timescales, http://dx.doi.org/10.1016/j.epsl.2013.03.014i.

Morimoto, M., O. Abe, H. Kayanne, N. Kurita, E. Matsumoto, and N. Yoshida (2002), Salinity records for the 1997-98 El Nino from Western Pacific corals, *Geophys. Res. Lett.*, *29*(11), 1540, doi:10.1029/2001GL013521.

Noone, D. (2006), Isotopic composition of water vapor modeled by constraining global climate simulations with reanalyses, *Rep*., pp. 2–37, World Meteorological Organization, Geneva, Switzerland.

Noone, D. (2012), Pairing measurements of the water vapor isotope ratio with humidity to deduce atmospheric moistening and dehydration in the tropical midtroposphere, *J. Climate*, *25*(13), 4476–4494.

Noone, D., and I. Simmonds (2002), Associations between $\delta^{18}O$ of water and climate parameters in a simulation of atmospheric circulation for 1979-95, *J. Climate*, *15*(22), 3150–3169.

Nurhati, I. S., K. M. Cobb, C. D. Charles, and R. B. Dunbar (2009), Late 20th century warming and freshening in the central tropical Pacific, *Geophys. Res. Lett.*, *36*, L21606, doi:10.1029/2009GL040270.

Partin, J. W., K. M. Cobb, J. F. Adkins, B. Clark, and D. P. Fernandez (2007), Millennial-scale trends in west Pacific warm pool hydrology since the Last Glacial Maximum, *Nature*, *449*(7161), 452–456.

Risi, C., S. Bony, and F. Vimeux (2008), Influence of convective processes on the isotopic composition ($\delta^{18}O$ and δD) of precipitation and water vapor in the tropics: 2. Physical interpretation of the amount effect, *J. Geophys. Res.*, *113*, D19306, doi:10.1029/2008jd009943.

Risi, C., S. Bony, F. Vimeux, L. Descroix, B. Ibrahim, E. Lebreton, I. Mamadou, and B. Sultan (2008b), What controls the isotopic composition of the African monsoon precipitation? Insights from event-based precipitation collected during the 2006 AMMA field campaign, *Geophys. Res. Lett.*, *35*, L24808, doi:10.1029/2008GL035920.

Risi, C., S. Bony, F. Vimeux, and J. Jouzel (2010), Correction to "Water-stable isotopes in the LMDZ4 general circulation model: Model evaluation for present-day and past climates and applications to climatic interpretations of tropical isotopic records", *J. Geophys. Res.*, *115*, D24123, doi:10.1029/2010JD015242.

Risi, C., et al. (2012), Process-evaluation of tropospheric humidity simulated by general circulation models using water vapor isotopic observations: 2. Using isotopic diagnostics to understand the mid and upper tropospheric moist bias in the tropics and subtropics, *J. Geophys. Res.*, *117*, D05304, doi:10.1029/2011JD016623.

Rozanski, K., L. Araguas-Araguas, and R. Gonfiantini (1993), Isotopic patterns in modern global precipitation, in *Climate Change in Continental Isotopic Records*, edited by P. K. Swart, pp. 1–36, American Geophysical Union, Washington, DC.

Sachs, J. P., D. Sachse, R. H. Smittenberg, Z. H. Zhang, D. S. Battisti, and S. Golubic (2009), Southward movement of the Pacific intertropical convergence zone AD 1400-1850, *Nat. Geosci.*, *2*(7), 519–525.

Schmidt, G. A., et al. (2006), Present-day atmospheric simulations using GISS ModelE: Comparison to in situ, satellite, and reanalysis data, *J. Climate*, *19*(2), 153–192.

Schmidt, G. A., A. N. LeGrande, and G. Hoffmann (2007), Water isotope expressions of intrinsic and forced variability in a coupled ocean-atmosphere model, *J. Geophys. Res.*, *112*, D10103, doi:10.1029/2006JD007781.

Sime, L. C., E. W. Wolff, K. I. C. Oliver, and J. C. Tindall (2009), Evidence for warmer interglacials in East Antarctic ice cores, *Nature*, *462*(7271), 342–U105.

Smith, T. M., R. W. Reynolds, T. C. Peterson, and J. Lawrimore (2008), Improvements to NOAA's historical merged land-ocean surface temperature analysis (1880-2006), *J. Climate*, *21*(10), 2283–2296.

Stewart, M. K. (1975), Stable isotope fractionation due to evaporation and isotopic exchange of falling waterdrops: Applications to atmospheric processes and evaporation of lakes, *J. Geophys. Res.*, *80*(9), 1133–1146 doi:10.1029/JC080i009p01133.

Sturm, C., Q. Zhang, and D. Noone (2010), An introduction to stable water isotopes in climate models: benefits of forward proxy modelling for paleoclimatology, *Clim. Past*, *6*(1), 115–129.

Thompson, L. G., E. Mosley-Thompson, H. Brecher, M. Davis, B. Leon, D. Les, P. N. Lin, T. Mashiotta, and K. Mountain (2006), Abrupt tropical climate change: Past and present, *Proc. Natl. Acad. Sci. U. S. A.*, *103* (28), 10536–10543.

Tierney, J. E., D. W. Oppo, Y. Rosenthal, J. M. Russell, and B. K. Linsley (2010), Coordinated hydrological regimes in the Indo-Pacific region during the past two millennia, *Paleoceanography*, *25*, PA1102, doi:10.1029/2009PA001871.

Tindall, J. C., P. J. Valdes, and L. C. Sime (2009), Stable water isotopes in HadCM3: Isotopic signature of El Niño-Southern Oscillation and the tropical amount effect, *J. Geophys. Res.*, *114*, D04111, doi:10.1029/2008JD010825.

Vuille, M., R. S. Bradley, M. Werner, R. Healy, and F. Keimig (2003), Modeling $\delta^{18}O$ in precipitation over the tropical Americas: 1. Interannual variability and climatic controls, *J. Geophys. Res.*, *108*(D6), 4174, doi:10.1029/2001JD002038.

Wu, H. C., and A. G. Grottoli (2010), Stable oxygen isotope records of corals and a sclerosponge in the Western Pacific warm pool, *Coral Reefs*, *29*(2), 413–418.

Xie, P. P., and P. A. Arkin (1997), Global precipitation: A 17-year monthly analysis based on gauge observations, satellite estimates, and numerical model outputs, *Bull. Am. Meteorol. Soc.*, *78*(11), 2539–2558.

Yoshimura, K., M. Kanamitsu, D. Noone, and T. Oki (2008), Historical isotope simulation using Reanalysis atmospheric data, *J. Geophys. Res.*, *113*, D19108, doi:10.1029/2008JD010074.